

# Pervasive *cis* effects of variation in copy number of large tandem repeats on local DNA methylation and gene expression

Paras Garg,<sup>1,3</sup> Alejandro Martin-Trujillo,<sup>1,3</sup> Oscar L. Rodriguez,<sup>1</sup> Scott J. Gies,<sup>1</sup> Elina Hadelia,<sup>1</sup> Bharati Jadhav,<sup>1</sup> Miten Jain,<sup>2</sup> Benedict Paten,<sup>2</sup> and Andrew J. Sharp<sup>1,\*</sup>

## Summary

Variable number tandem repeats (VNTRs) are composed of large tandemly repeated motifs, many of which are highly polymorphic in copy number. However, because of their large size and repetitive nature, they remain poorly studied. To investigate the regulatory potential of VNTRs, we used read-depth data from Illumina whole-genome sequencing to perform association analysis between copy number of ~70,000 VNTRs (motif size  $\geq 10$  bp) with both gene expression (404 samples in 48 tissues) and DNA methylation (235 samples in peripheral blood), identifying thousands of VNTRs that are associated with local gene expression (eVNTRs) and DNA methylation levels (mVNTRs). Using an independent cohort, we validated 73%–80% of signals observed in the two discovery cohorts, while allelic analysis of VNTR length and CpG methylation in 30 Oxford Nanopore genomes gave additional support for mVNTR loci, thus providing robust evidence to support that these represent genuine associations. Further, conditional analysis indicated that many eVNTRs and mVNTRs act as QTLs independently of other local variation. We also observed strong enrichments of eVNTRs and mVNTRs for regulatory features such as enhancers and promoters. Using the Human Genome Diversity Panel, we define sets of VNTRs that show highly divergent copy numbers among human populations and show that these are enriched for regulatory effects and preferentially associate with genes that have been linked with human phenotypes through GWASs. Our study provides strong evidence supporting functional variation at thousands of VNTRs and defines candidate sets of VNTRs, copy number variation of which potentially plays a role in numerous human phenotypes.

## Introduction

Tandem repeats (TRs) are stretches of DNA comprised of two or more contiguous copies of a sequence of nucleotides arranged in head-to-tail pattern, e.g., CAG-CAG-CAG. The human genome contains >1 million TRs that collectively span ~3% of our total genome.<sup>1</sup> These TRs range in motif size from mono-nucleotide repeats at one extreme (e.g., TTTT) to those with much larger motifs that can in some cases be several kilobases in size, even containing entire exons or genes within each repeated unit.<sup>2,3</sup> Because of their repetitive nature, TRs often show high mutation frequencies, and many show extremely high levels of length polymorphism.<sup>4,5</sup> For example, a recent comprehensive study of genome variation showed that ~50% of insertion-deletion events within the human genome map to TR regions.<sup>6</sup> However, despite contributing to a large fraction of genetic variation, TRs remain poorly studied and, as a result, their influence on human phenotypes is almost certainly underestimated. This is largely due to their repetitive and highly variable nature, which until the recent advent of specialized algorithms designed to genotype TR lengths from sequencing data, made them largely inaccessible to high-throughput genotyping approaches.<sup>7–12</sup>

Previously, we and others have demonstrated functional effects on local gene expression and epigenetics of length variation in TRs with both short motifs (motif size 1–6 bp, often termed microsatellites) and TRs with very large motifs (motif size > 2 kb, also termed macrosatellites).<sup>13–16</sup> In contrast, TRs with motif sizes between these two extremes, often termed variable number tandem repeats (VNTRs) or minisatellites, have been less well studied. This is largely due to technical difficulties of genotyping variation at loci composed of moderate-to-large tandem repeats motifs and is further compounded by the fact that many TRs undergo a relatively high rate of recurrent mutation, meaning that copy number variation of large TRs is often poorly tagged by flanking SNVs.<sup>16</sup> As a result, variation of many TR loci is poorly ascertained by standard SNV-based genome-wide association studies (GWASs). Thus, there is currently a knowledge gap regarding the role of TR variation in human disease.

Numerous targeted studies in the literature have implicated length variation of VNTR loci as putative drivers of human molecular and disease phenotypes. Specific examples include a 12-mer repeat upstream of *CSTB* (MIM: 601145) that is the strongest known expression quantitative trait locus (eQTL) associated with *CSTB* expression; a 30-mer repeat in the promoter of *MAOA* (MIM: 309850)

<sup>1</sup>Department of Genetics and Genomic Sciences and Mindich Child Health and Development Institute, Icahn School of Medicine at Mount Sinai, New York, NY 10029, USA; <sup>2</sup>UC Santa Cruz Genomics Institute, University of California, Santa Cruz, Santa Cruz, CA 95064, USA

<sup>3</sup>These authors contributed equally

\*Correspondence: [andrew.sharp@mssm.edu](mailto:andrew.sharp@mssm.edu)

<https://doi.org/10.1016/j.ajhg.2021.03.016>

© 2021 American Society of Human Genetics.



implicated in multiple neurologic and behavioral phenotypes; a 14-mer repeat upstream of *INS* (MIM: 176730) that is associated with multiple metabolic traits, insulin production, and diabetes risk; and an 25-mer repeat intronic within *ABCA7* (MIM: 605414) that is enriched for long alleles in Alzheimer disease and correlates with *ABCA7* splicing and amyloid  $\beta$  levels in cerebrospinal fluid.<sup>17–22</sup>

Building on this prior work, here we used read depth from Illumina whole-genome sequencing (WGS) data to perform a genome-wide analysis of copy number variation at  $\sim 70,000$  VNTR loci (defined here as TRs that have motif size  $\geq 10$  bp and span  $\geq 100$  bp in the reference genome) in two discovery cohorts and a third replication population. Our study provides functional insight into a previously understudied fraction of human genetic variation and suggests that future studies of VNTR variation may explain some of the “missing heritability” of the human genome.<sup>23,24</sup>

## Subjects and methods

### Description of cohorts used for VNTR association analysis

Individuals included in this study provided proper informed consent for research use, and all procedures followed were in accordance with the ethical standards of the responsible committee(s) on human studies. Local ethical approval for this study was granted under HS#: 20-00153.

#### GTE<sub>x</sub>

We obtained Illumina 150 bp paired-end WGS data and resulting variant calls made with GATK in 620 individuals from the Genotype-Tissue Expression (GTEx) project from dbGAP (dbGAP: phs000424.v7.p2). Normalized RNA sequencing (RNA-seq) expression data for these samples were downloaded from the GTEx portal (v.7), comprising quality-controlled and processed files for 48 tissues generated by the GTEx Consortium. These data were aligned to hg19 and had already undergone filtering to remove genes with low expression and been subject to rank-based inverse normal transformation.

#### PCGC

WGS and methylation data for 249 individuals were selected from the cohort collected by the Pediatric Cardiac Genomic Consortium (PCGC). An extensive description of PCGC samples as well as further details about sample collection can be found in a summary publications released by the PCGC.<sup>25,26</sup> Briefly, the cohort comprises individuals aged from newborn to 47 years (mean 8.2 years) diagnosed with a range of congenital heart defects; conotruncal and left-sided obstructive lesions were the two most common diagnoses. Illumina 150 bp paired-end WGS data generated via PCR-free libraries from peripheral blood DNA (average of  $36\times$  genome coverage, range 25– $39\times$ ) were obtained from dbGAP (dbGAP: phs001138.v1.p2). Peripheral blood methylomes were downloaded from GEO (GEO: GSE159930) and normalized as described previously.<sup>27</sup> We utilized the array data to infer the likely sex of each sample on the basis of scatterplots of mean  $\beta$  value of probes located on the X chromosome (chrX) versus the fraction of probes located on the Y chromosome (chrY) with detection  $p > 0.01$ . We compared these predictions against self-reported sex for each sample and removed four sam-

ples with a potential sex mismatch. We utilized data from autosomal probes, excluding any that mapped to multiple genomic locations. We also utilized the genotypes obtained from GATK analysis of the WGS data and in each sample excluded  $\beta$  values for any CpG that contained an SNV within either the probe-binding site or the interrogated CpG. After these filters, a total of 821,035 CpG sites were retained for downstream analysis. All PCGC data were aligned to hg19.

#### PPMI

We utilized data from the Parkinson's Progression Markers Initiative (PPMI) cohort, corresponding to 712 individuals (189 healthy control individuals and 523 affected individuals with varying types of Parkinsonism), with available Illumina WGS data aligned to the hg38 reference genome.<sup>28</sup> RNA-seq data generated from peripheral blood were available for 676 PPMI samples, comprising read counts for 22,582 genes listed in GENCODE v.19, aligned to hg19. The read counts were filtered, normalized, and subjected to rank-based inverse normal transformation via scripts provided by the GTEx Consortium. DNA methylation data generated via the Illumina 850k array from peripheral blood DNA were available for 524 PPMI samples, aligned to hg19.

### Estimation of VNTR copy number in two discovery cohorts

We downloaded 886,954 autosomal TRs listed in the simple repeats track from the hg19 build of the UCSC Genome Browser, retaining only those repeats with motif size  $\geq 10$  bp and total length of repeat tract  $\geq 100$  bp. Where multiple TR annotations overlapped, these were merged together, resulting in 89,893 unique autosomal VNTR regions that were used in subsequent analysis. All analyses in GTEx and PCGC discovery cohorts were performed with the hg19 assembly.

In each sample of the discovery cohort (GTEx and PCGC), we estimated relative diploid copy number of each autosomal VNTR region by using CNVnator (v.0.3.3 with default thresholds and bin size 100 bp), which uses normalized read depth to estimate copy number of a locus.<sup>29</sup> It should be noted that in VNTR regions, where by definition there are multiple copies of a repeated motif, CNVnator copy number estimates represent the fold change in total (diploid) repeat number relative to the number of motifs annotated in the (haploid) reference genome. For example, Figure 1A shows CNVnator-estimated copy number for a 44-mer repeat that has 43 copies in the reference genome (chr12: 132,148,891–132,150,764, hg38). An individual with a relative CNVnator copy estimate of 6 is therefore predicted to carry a total of  $43 \times 6 = 258$  copies of this repeat.

Utilizing CNVnator copy number estimates of invariant regions of the genome, we observed a strong technical bias in GTEx WGS data: samples that were sequenced prior to 2016 showed systematic shifts in estimated copy number compared with later batches (Figure S1). As a result, we removed 136 samples that were sequenced in batch “2015-10-06.” On the basis of analysis of invariant loci, and principal component analysis and density plots based on VNTR copy number, we excluded a further 60 samples from the GTEx cohort and 10 samples from the PCGC cohort that were outliers in one or more of these analyses (Figure S2).

In situations where a VNTR is embedded within a larger copy number variable region, copy number estimates for a VNTR based on read depth can be confounded by variations of the wider region because these would result in gains or losses in the total number of VNTR copies present but without any change in the length of the

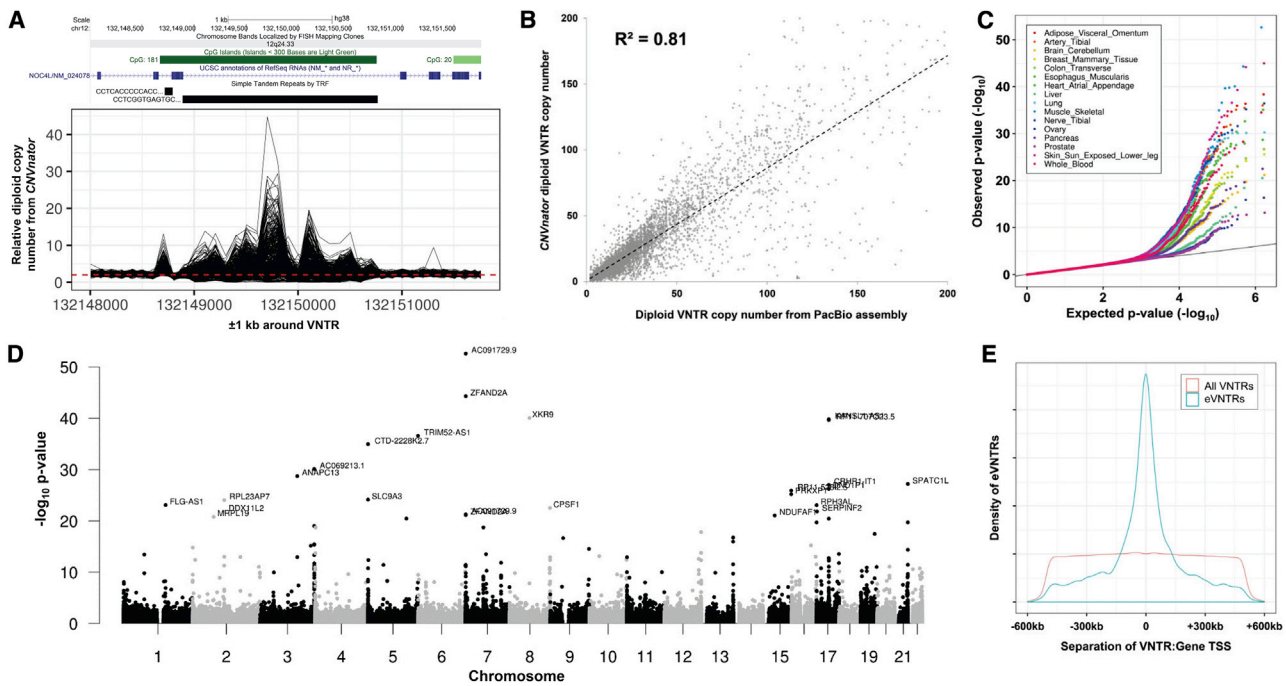


**Figure 1. Copy number variation at thousands of VNTRs is associated with variation in gene expression and DNA methylation in *cis*** (A) CNVnator-estimated copy number per 100 bp bin over a VNTR region shows highly variable read depth among samples from the GTEx cohort. Shown is read depth data for a 44-mer repeat that has 43 copies in the reference genome (chr12: 132,148,891–132,150,764, hg38), located intronic within *NOC4L*, which shows >10-fold difference in copy number within the population. (B) Read depth provides good accuracy for estimating diploid VNTR copy number. Using 14 samples where both Illumina and PacBio WGS data were available, at 1,891 eVNTR loci we compared diploid VNTR copy number estimates from WGS read depth by using CNVnator with direct genotypes derived from Pacific Biosciences long-read diploid assemblies. We observed a high correlation between the two approaches ( $R^2 = 0.81$ ). (C) Q-Q plots showing the distribution of observed versus expected p values for eVNTRs in 16 representative GTEx tissues. Variations in the observed p value distribution among GTEx tissues are a reflection of the varying sample sizes available, which strongly influence statistical power. (D) Manhattan plot showing results of *cis*-association analysis between VNTR copy number and gene expression in skeletal muscle samples from the GTEx cohort. The high frequency of significant associations in subtelomeric and centromeric regions is consistent with the known enrichment of VNTRs in these regions.<sup>30,31</sup> (E) Significant eVNTRs are highly enriched within close proximity to the genes whose expression level they are associated with, mirroring similar observations made for SNV eQTLs.<sup>32,33</sup> We also observed a similar relationship for mVNTRs and the CpGs they associate with (Figure S10), although we note an approximate order of magnitude difference in the distances over which significant eVNTRs and mVNTRs were typically observed to function.

VNTR array. To identify VNTRs where our copy number estimates were potentially subject to this confounder, we performed copy number analysis of the 3' and 5' regions flanking each VNTR by using CNVnator (Figure S3). In cases where the 1 kb flanking region of a VNTR overlapped a simple repeat with motif size  $\geq 6$  bp, we trimmed the flanking region, retaining only the flanking portion that was adjacent to the VNTR. We then removed from our analysis any VNTRs where

- (1) both flanks had trimmed length < 500 bp;
- (2) correlation ( $R$ ) between copy number of the VNTR and either of the flanking regions was  $>0.5$ ;
- (3) either flanking region showed large variations in copy number, defined as those flanks where the difference between 99<sup>th</sup> and 1<sup>st</sup> percentile was  $>2$ ;
- (4) they overlapped CNVs with minor allele frequency  $> 10\%$  in Europeans.<sup>34</sup>

As copy number estimates in GTEx WGS samples showed high variability based on analysis of density plots, we normalized

VNTR copy numbers in the 424 remaining samples by applying an inverse rank normal transformation.<sup>35</sup> On the basis of visual inspection of density plots of these transformed copy numbers, we removed a further 20 outlier samples (Figure S2), leaving 404 samples that were used for association analysis with gene expression (Table S1). Finally, we removed VNTRs that showed very low levels of variation in the population (standard deviation  $< 0.2$ ).

### Comparison of VNTR copy number estimates with genotypes obtained via long reads and the advNTR algorithm

Using the tool MsPAC, we generated diploid genome assemblies for 14 individuals from available Pacific Biosciences (PacBio) WGS data and phased SNVs (Table S2).<sup>36</sup> Where phased SNVs were not available (samples HG02059, HG02818, HG03486, and HG0386), we performed phasing by using GATK HaplotypeCaller and WhatsHap.<sup>37</sup> We generated VNTR genotypes directly from the diploid long-read assemblies by using PacMonSTR.<sup>38</sup> For each of these individuals, PCR-free Illumina WGS data were also available,

and we processed them with CNVnator to estimate VNTR copy number, as described above. To estimate the accuracy of our VNTR genotypes derived via CNVnator, we utilized a set of 2,027 VNTRs that are associated with local gene expression (eVNTRs) that showed significant associations with gene expression in one or more GTEx tissues and that were composed of single annotated (i.e., non-merged) tandem repeats, copy number of which could be unambiguously genotyped with PacMonSTR. We discarded genotypes where both haplotypes in a sample were not represented in the PacBio genome assemblies or where VNTR copy number was >200, yielding a final total of 16,403 pairwise genotypes derived from 1,891 VNTR loci across the 14 samples, representing all eVNTR loci genotyped by CNVnator for which we also obtained at least one set of diploid genotypes from the 14 PacBio genome assemblies analyzed. To assess the performance of an alternative approach for genotyping VNTRs from short-read WGS, we were also able to generate genotypes for 1,746 of these same 1,891 loci from the Illumina WGS reads with advNTR in the 14 samples by using default parameters.<sup>11</sup>

### Identification of eVNTRs in the GTEx cohort

Using RNA-seq data from the filtered set of 404 WGS samples that passed our quality control steps, we adjusted gene expression data for sex, RNA-seq platform, the first three principal components from SNV genotypes, and between 15–60 covariates per tissue estimated via PEER.<sup>39</sup> Within each tissue, we performed linear regression between VNTR copy number and corrected expression level of each gene located within  $\pm 500$  kb by using the `lm` function in R. We applied a false discovery rate (FDR) correction and reported all VNTR:gene pairs with  $FDR\ q < 0.1$  in any tissue.<sup>40</sup>

### Identification of mVNTRs in the PCGC cohort

After excluding samples that either did not pass our quality control for DNA methylation or were outliers for VNTR copy number on the basis of density plots, 235 individuals from the PCGC cohort were utilized for association analysis of VNTR copy number with CpG methylation levels (VNTRs that are associated with DNA methylation levels, or mVNTRs). We excluded CpGs with low levels of variation (standard deviation < 0.02), leaving 316,169 CpGs that were located within  $\pm 50$  kb of VNTRs that were used for association analysis. CpG methylation data ( $\beta$  values) were adjusted for age, sex, the top two ancestry-related principal components derived from principal-component analysis (PCA) of SNVs, and blood cell fractions estimated directly from the methylation data with the Houseman method.<sup>41,42</sup> We used the resulting residuals to test the association between DNA methylation and estimated VNTR copy number by using the `lm` function in R. We applied a Bonferroni correction to the resulting p values based on the total number of pairwise VNTR:CpG tests performed and considered those with Bonferroni-adjusted  $p < 0.01$  as significant.

### Replication of eVNTRs and mVNTRs in the PPMI cohort

We utilized available WGS, RNA-seq and methylation data for 712 individuals from the PPMI cohort. We generated copy number estimates for all VNTR loci utilized in the GTEx and PCGC discovery cohorts by using CNVnator (v.0.4.1) and applied the same quality control and normalization steps as used in the discovery cohorts, including inverse rank normal transformation to the VNTR copy numbers, resulting in the exclusion of nine outlier samples. We normalized gene expression data by using the same method as applied to the GTEx cohort, including application of inverse

rank normal transformation. These normalized expression data were adjusted for sex, the first three ancestry-related principal components derived from PCA of SNVs, and 60 additional components estimated via PEER.<sup>39</sup> We performed association between VNTRs and normalized adjusted gene expression levels by using linear regression, as described above for the GTEx cohort.

For replication of mVNTRs, we applied the same quality control and normalization pipeline to the methylation data as used for the PCGC cohort, as described above. Normalized  $\beta$  values were adjusted for sex, age, the top three principal components from SNV genotypes, and estimated blood cell fractions. We then used the residuals to perform linear regression with VNTR genotype. CNVnator analysis of the PPMI cohort was performed in the hg38 assembly, and we used `liftOver` to convert VNTR coordinates to the hg19 assembly for association analysis with methylation and expression data.

### Enrichment analysis

We performed all enrichment analyses by comparing the frequency of significant eVNTRs and mVNTRs against the background set of all VNTR:gene pairs that were tested in each cohort, and we generated p values by using the hypergeometric distribution. We defined promoter regions as  $\pm 2$  kb of gene transcription start sites (TSSs). We utilized a set of enhancer element annotations downloaded the GeneHancer track in the UCSC Genome Browser, utilizing only loci labeled “Enhancers.”<sup>43</sup> We utilized a composite list of silencer element annotations, corresponding to all significant silencer elements identified in two cell types under different conditions.<sup>44</sup>

### Replication of VNTR:CpG associations via Oxford Nanopore long-read data

FASTQ files with Oxford Nanopore technology (ONT) reads-derived WGS from 30 EBV-transformed lymphoblastoid cell lines were downloaded from the Human Pangenome Reference Consortium and aligned to hg38 via `minimap2` with default parameters.<sup>45</sup> SNV calls were generated for each sample via the `bwa-GATK` pipeline based on Illumina WGS downloaded from the International Genome Sample Resource. Variants were phased with `WhatsHap`<sup>37</sup> and the alignment of the ONT reads to the reference genome. We generated diploid genome assemblies by using `MsPAC`<sup>36</sup> with ONT reads aligned to hg38 and phased SNVs as input. VNTRs were genotyped on each assembled haplotype via `PacMonSTR`.<sup>38</sup> We used the `call-methylation` function in `nanopolish` to score CpG sites in each read as either methylated or not methylated.<sup>46</sup> Because `MsPAC` partitioned reads into the two possible haplotypes per sample, we calculated the methylation fraction for each CpG site per haplotype on the basis of all haplotype-phased reads overlapping each CpG. In order to ensure robust methylation measurements, we only retained CpGs for phased haplotypes that were covered by  $\geq 10$  reads. We then calculated correlation coefficients between VNTR copy number and methylation fractions for mVNTR:CpG pairs identified in the PCGC cohort where there were  $\geq 20$  haplotypes with both VNTR genotypes and CpG measurements available and where the VNTR showed an allelic range  $\geq 2$  copies.

### Population stratification of VNTRs

We obtained Illumina WGS reads mapped to hg38 from samples in the Human Genome Diversity Panel, utilizing data for a subset of 676 samples that were sequenced with PCR-free protocols.<sup>47</sup> We

used CNVnator (v.0.4.1) to estimate relative copy number of autosomal VNTRs (hg38). We performed quality control by using PCA and density plots to remove outliers and compared the reported sex of each sample against sex chromosome copy number, removing any discordant samples. We filtered VNTRs to remove those within putative larger CNVs, as detailed above. After applying these filters, we utilized genotypes of 66,796 VNTRs in 643 samples from seven different super-populations. For each super-population, we calculated  $V_{ST}$  as follows:

$$V_{ST} = (V_A - ((C_T \times V_T) + (C_B \times V_B)))/V_A,$$

where  $V_A$  is the variance of all the samples,  $V_T$  is the variance of the target population,  $V_B$  is the variance of the background population, and  $C_T$  and  $C_B$  are fractions of the number of target and background populations, respectively.<sup>48</sup> For each of the seven super-populations, we calculated  $V_{ST}$  for each VNTR by considering one super-population as the target and using all other samples as background.  $p$  values were generated by permutation testing ( $n = 1,000$  permutations), and samples were randomly assigned to either the target or background groups. We selected those VNTRs in each super-population with  $V_{ST} \geq 0.1$  and permutation  $p < 0.01$ .

### Annotation of VNTRs with potential trait associations

In order to link eVNTRs with human traits that they might influence, we used two complementary approaches. First, we used results of PrediXcan applied to 44 GTEx tissues and >100 phenotypes from GWASs, annotating eVNTRs with phenotypes if they shared the same gene name and tissue as indicated by PrediXcan.<sup>49</sup> However, because PrediXcan has been applied to a relatively limited set of traits, we further annotated eVNTRs by using a combination of eQTLs identified by the GTEx project and SNVs from the GWAS Catalog.<sup>50</sup> Here, eVNTRs were linked to putative associated phenotypes as follows: (1) for each eVNTR identified in a specific tissue, we joined these with eQTLs identified in the same GTEx tissue based on gene name; (2) we extracted all SNVs from the GWAS Catalog with  $p < 5 \times 10^{-8}$  and joined these to the GTEx eQTLs; and (3) where an eVNTR was joined with an SNV that was both a GWAS variant and an eQTL for the same gene in the same tissue, we annotated the eVNTR with the GWAS phenotype(s).

### Analysis of eVNTRs and mVNTRs on the X chromosome

Although all analysis described above was based on autosomal loci, we also performed association analysis of VNTRs on the X chromosome in the GTEx, PCGC, and PPMI cohorts. Here, we only analyzed 46,XY males, as determined by read-depth analysis of the sex chromosomes ( $n = 182$  in GTEx,  $n = 123$  in PCGC, and  $n = 465$  in PPMI). After removal of the pseudo-autosomal regions and quality filtering (as described above), we performed association analysis of 2,348 VNTRs with gene expression and DNA methylation, utilizing the same statistical thresholds as for autosomal loci.

## Results

### Robust genotyping of VNTRs via read depth

Using read depth from Illumina WGS data as a proxy for diploid copy number, we generated copy number estimates for a set of 70,787 large TRs (median motif size

116 bp, mean span of repeat tract in reference genome 353 bp), henceforth referred to as variable number tandem repeats (VNTRs). Many VNTR loci showed highly variable copy number estimates among different individuals, indicative of extreme levels of inter-individual polymorphisms at many of these loci (Figure 1A).

In order to assess the validity of genotyping VNTRs from read depth, we compared estimated VNTR copy numbers from CNVnator with genotypes obtained directly from spanning long reads from *de novo* diploid PacBio genome assemblies. Using 14 individuals for which both Illumina and PacBio WGS data were available, we observed good global correlation between these two approaches, with an overall  $R^2 = 0.81$ , indicating that read depth is generally an effective proxy for measuring total copy number at the majority of VNTR loci (Figure 1B, Table S3). In comparison, we found that an alternative tool designed for genotyping VNTRs from short-read data performed relatively poorly, yielding an  $R^2 = 0.14$  when compared with direct genotypes generated from long-read WGS (Figure S4, Table S3).<sup>11</sup>

Given that some VNTR motifs are not unique and can occur at multiple genomic loci, we investigated the reliability of reads mapped to VNTR loci. Using high-coverage Illumina WGS data in a Yoruba individual from the 1000 Genomes Project (NA18874), we assessed mapping quality scores for reads that overlapped VNTRs on the basis of both their MAPQ score and the MAPQ score of their mate pairs. We classified reads from VNTR loci into three categories. The first category was  $MAPQ \geq 10$ , which we considered reliably mapped. The second category was  $MAPQ < 10$  but with a mate pair that mapped reliably within  $\pm 10$  kb. We considered these reads as reliably mapped to the correct VNTR on the basis of their mate pair. Likely many such reads that are contained entirely within a VNTR yield low mapping quality because of the fact that VNTRs are composed of repeated copies, giving multiple possible map positions within a single VNTR tract. The third category was  $MAPQ < 10$  and with a mate pair that was not anchored within  $\pm 10$  kb. We considered these reads unreliably mapped. Overall, we observed that the vast majority of reads from VNTR loci were reliably mapped: 97.5% of VNTRs comprised <10% of overlapping reads that were unreliably mapped ( $MAPQ < 10$  and no anchoring mate pair), and only a single VNTR contained >50% of unreliably mapped reads (Figure S5). These data indicate that ambiguous read mapping to tandemly repeated regions is not a significant confounder of our approach.

### Overview of association analysis of VNTRs with gene expression and DNA methylation

To assess the potential regulatory effects of copy number changes of VNTRs on local gene expression and epigenetics we utilized two discovery cohorts for which PCR-free Illumina WGS data were available. First, we used a subset of quality-filtered samples from the GTEx project, comprising 404 individuals with expression data from

48 different tissues. Here, we performed *cis*-association analysis between estimated VNTR copy number and normalized gene expression within  $\pm 500$  kb. Second, we used 235 quality-filtered samples from the PCGC for which DNA methylation profiles from whole blood were available. Here, we performed *cis*-association analysis between estimated VNTR copy number and CpG methylation levels within  $\pm 50$  kb.

### Summary of autosomal gene expression associations in the GTEx cohort

After multiple testing correction, in the GTEx cohort we identified a total of 13,752 significant pairwise VNTR:gene expression associations (10% FDR) across 48 different tissues, corresponding to 2,980 unique expression QTL VNTRs (henceforth termed eVNTRs) that were associated with the expression level of 3,167 different genes (Table S4). Using Q-Q plots to explore the distribution of observed versus expected associations, in each GTEx tissue we observed a clear enrichment for significant associations compared with the null distribution and little evidence of genomic inflation (mean  $\lambda = 1.019$ , range 0.997–1.040) (Figure 1C). As expected, the number of significant associations observed in different tissues was strongly associated with sample size (i.e., statistical power), varying from 13 identified in uterus to 1,080 in thyroid (Table S4). An example of the distribution of genome-wide association signals observed in skeletal muscle is shown in Figure 1D. Of note, we frequently observed the same VNTR:gene pairwise associations in multiple different tissues (35% of VNTR:gene associations were seen in  $\geq 2$  tissues), and of these, 99.4% showed consistent directionality in different tissues (Figure S6, Table S4). In addition, 34% of eVNTRs were associated with the expression of multiple different genes (mean of 3 associated genes per eVNTR, range 1–48).

Supporting a biological role in modulating gene expression, eVNTRs showed enrichments for several genome annotations with regulatory potential. We observed a 7.9-fold enrichment for eVNTRs located within  $\pm 2$  kb of transcription start sites ( $p = 1.1 \times 10^{-73}$ , Figure 1E). Consistent with this observation, the sequence content of eVNTRs also showed a strong bias toward higher GC content (permutation  $p < 10^{-7}$ ) (Figure S7). We also observed that eVNTRs were enriched at both annotated enhancer (1.7-fold enrichment,  $p = 1.7 \times 10^{-14}$ ) and silencer elements (2.5-fold enrichment,  $p = 1.9 \times 10^{-4}$ ). Further examples of results observed at eVNTRs in the GTEx cohort are shown in Figure S8.

In further support of our results, we successfully replicated three associations of VNTRs with the expression level of individual genes that had been identified in previous targeted studies: a 36-mer coding VNTR in exon 1 of *AS3MT* (MIM: 611806) that is associated with *AS3MT* expression and schizophrenia risk, a 72-mer intronic VNTR that regulates *SIRT3* expression (MIM: 604481), and a 33-mer promoter VNTR that regulates expression

of *TRIB3* (MIM: 607898), a gene that has been linked with multiple human phenotypes.<sup>51–53</sup>

### Summary of autosomal DNA methylation associations in the PCGC cohort

As for eVNTRs in the GTEx cohort, a Q-Q plot showed a clear enrichment for significant associations compared with the null distribution, although with some evidence for genomic inflation ( $\lambda = 1.297$ ) (Figure S9). Because of this, in order to ensure robust associations, we chose to apply a more stringent multiple testing correction, identifying a total of 3,152 VNTR:CpG pairwise associations in the PCGC cohort (Bonferroni-corrected  $p < 0.01$ ), corresponding to 1,480 unique methylation QTL VNTRs (henceforth termed mVNTRs) and 2,466 unique CpGs (Table S5). Similar to observations made for eVNTRs, mVNTRs also showed a strong bias to occur in close proximity to the CpGs they associated with, and the majority are separated by  $< 5$  kb (Figure S10). mVNTRs tended to have a significantly higher GC content than all VNTRs in the genome (permutation  $p < 10^{-7}$ , Figure S7) and were 2.2-fold enriched for annotated enhancers ( $p = 3.7 \times 10^{-19}$ ) and 2.2-fold enriched for annotated silencers ( $p = 8.1 \times 10^{-3}$ ). Three examples of the association signals observed around mVNTRs are shown in Figure 2, while additional plots of eight other mVNTR loci are shown in Figure S11.

### Conditional analysis indicates many VNTR associations are independent of SNV QTLs

Given that multiple different genetic variants may exert regulatory effects on gene expression and CpG methylation, we considered the possibility that the VNTR associations we observed might be indirect correlations driven by linkage disequilibrium between VNTRs and other variants that are the primary QTLs. To assess whether VNTRs act as QTLs independent of other local genetic variation, we performed conditional analyses by removing the effect of the strongest SNV QTL associated with each gene and CpG that were putatively associated with VNTR copy number.

First, we utilized SNV genotypes from the WGS data in our two discovery cohorts to identify SNVs that were significantly associated (FDR  $q < 0.1$ ) with local gene expression and CpG methylation levels (Figure 3A). For each VNTR pairwise association, we then retained only the subset of individuals that were homozygous for the major allele of the lead QTL SNV and repeated the association analysis between VNTR copy number and gene expression/DNA methylation (Figure 3B). Doing so, we observed a clear trend where the majority of VNTR associations retained the same directionality as in our original analyses (Figures 3C and 3D). Overall, 9,791 of 12,784 eVNTR:gene pairs (76.6%) and 2,280 of 3,152 mVNTR:CpG pairs (72%) showed the same direction of association after conditioning on the lead QTL SNV. Despite a considerable loss of statistical power due to the reduced sample size when conditioning based on the strongest SNV QTL, in

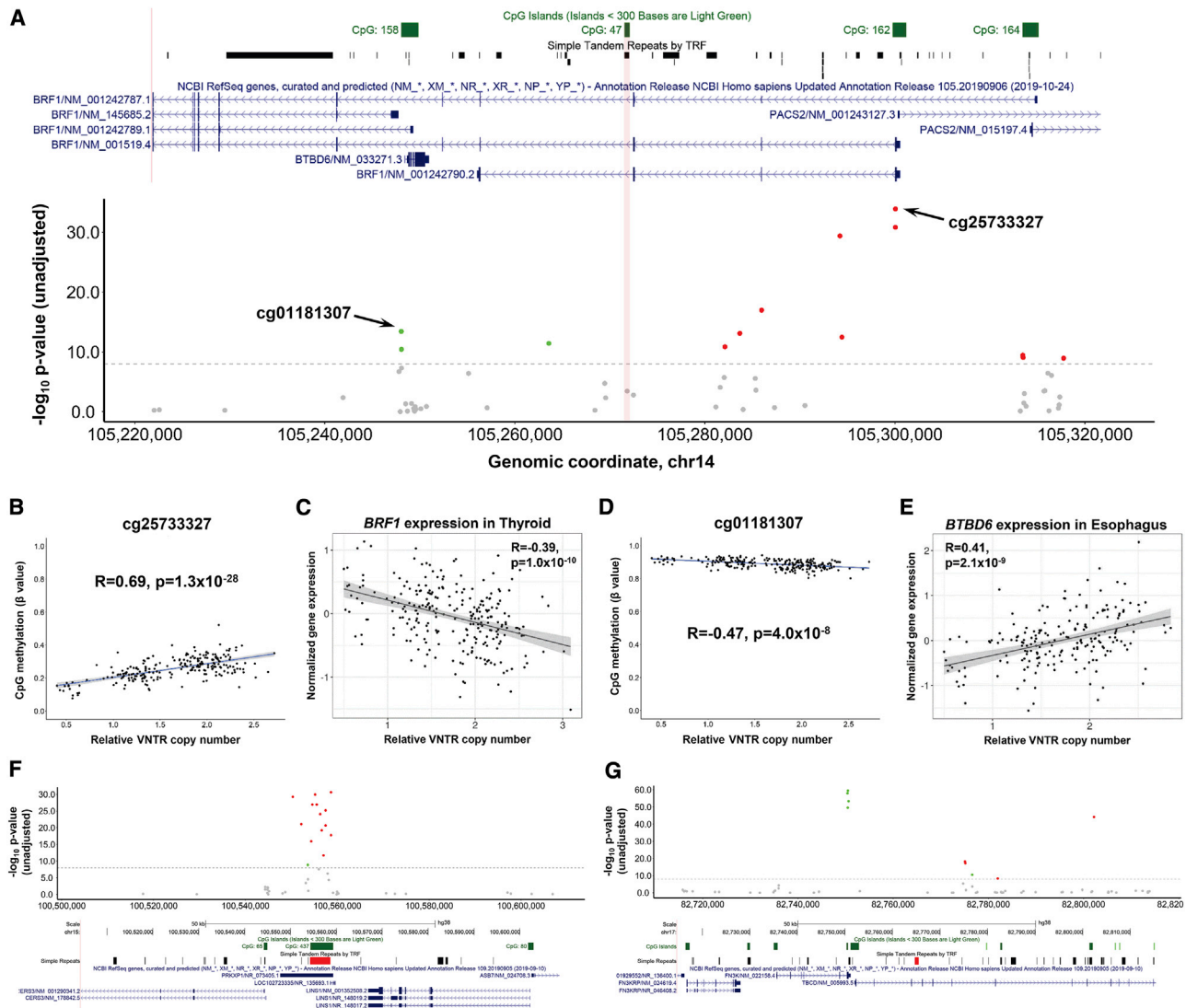


**Figure 2. Example associations of VNTRs with *cis*-linked DNA methylation and gene expression**

Copy number of a 72-mer tandem repeat (chr14: 105,271,805–105,272,305, hg38) is associated with DNA methylation levels at multiple CpGs spread over >80 kb and the expression of multiple genes in *cis*.

(A) Manhattan plot of associations between copy number of this VNTR and CpG methylation within  $\pm 50$  kb. Significant CpGs ( $p < 0.01$  after Bonferroni correction for the number of pairwise tests performed genome wide) are shown in color: red represents positive correlations with VNTR copy number and green indicates negative correlations. The location of the 72-mer VNTR is indicated by the vertical red bar in the center of the plot. The dashed gray line indicates the Bonferroni significance threshold. Above the plot is an image from the UCSC Genome Browser showing location of CpG islands, simple repeats, and RefSeq genes.

(B and C) Correlation of VNTR copy number with CpG methylation (cg25733327) that lies 1 kb downstream of the TSS of *BRF1* and expression of *BRF1* in thyroid.

(D and E) Correlation of VNTR copy number with CpG methylation (cg01181307) that lies 500 bp upstream of the TSS of *BTBD6* and expression of *BTBD6* in esophagus muscularis. For both genes, increased methylation levels around the TSS are associated with reduced gene expression, which is consistent with the known repressive effects of promoter methylation.

(F) A 107-mer repeat (chr15: 100,554,293–100,558,659, hg38), increased copy number of which causes local hypermethylation. This VNTR also associates with the expression level of multiple nearby genes in many different tissues.

(G) A 40-mer repeat (chr17: 82,764,738–82,765,449, hg38), which associates with methylation of multiple CpGs over an  $\sim 50$  kb region. This VNTR also associates with the expression level of multiple nearby genes in many different tissues. In (F) and (G), the location of the associated VNTR is shown by a red bar in the simple repeats track.

the GTEx cohort, 2,146 associations showed the same direction of effect with  $p < 0.01$  and 1,434 met our genome-wide significance discovery threshold (FDR  $q < 0.1$ ) (Table S4). Similarly, for mVNTRs identified in the PCGC cohort, after conditioning on the lead mQTL SNV, 693 associations showed the same direction of effect with

$p < 0.01$  and 273 associations met our genome-wide significance discovery threshold (Bonferroni  $p < 0.01$ ) (Table S5). Overall, these results indicate that many of the VNTR associations we detected are independent of other local QTLs and are not simply driven by the linkage disequilibrium architecture of the genome.

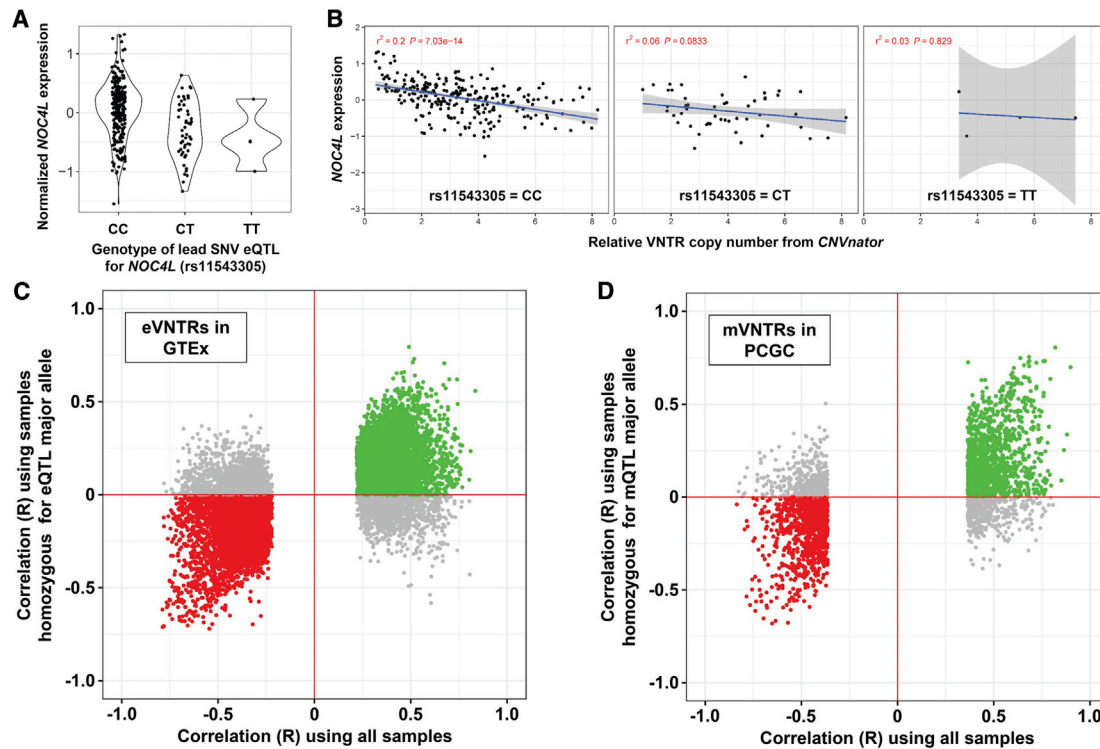


**Figure 3. Copy number variation at the majority of VNTRs shows association with gene expression and DNA methylation independently of SNV eQTLs and mQTLs**

We performed conditional analysis of eVNTRs and mVNTRs after removing the effect of the strongest SNV QTL on the same target. Shown is an example locus, a 44-mer repeat that has 43 copies in the reference genome (chr12: 132,148,891–132,150,764, hg38), corresponding to the same VNTR shown in Figure 1A. This VNTR is located intronic within *NOC4L* and is significantly associated with *NOC4L* expression.

(A) We identified rs11543305, a C/T variant that is located 1.6 kb proximal to the VNTR, as being the lead SNV associated with *NOC4L* expression.

(B–D) After stratifying samples on the basis of genotype at rs11543305, copy number of this VNTR still shows a significant association with *NOC4L* expression (B). Considering all significant VNTRs we identified, including eVNTRs observed in GTEx (C) and mVNTRs observed in the PCGC cohort (D), there is a clear trend where the majority of observed VNTR associations retain their original signal even after conditioning on the genotype of the lead SNV QTL. These data indicate that the majority of VNTR associations we identified act independently of local SNV QTLs. In each plot, colored points represent VNTR associations that retain the same directionality after conditioning on the lead SNV QTL: either positive associations (green) or negative associations (red).

### Large-scale replication of eVNTRs and mVNTRs in an independent cohort

In order to assess the robustness of the associations we identified in the GTEx and PCGC discovery cohorts, we conducted replication analysis in the PPMI cohort, consisting of a total of 703 individuals with WGS, gene expression, and methylation data. We used CNVnator to analyze VNTR copy number in each sample and then performed association analysis with both gene expression and CpG methylation levels by using identical pipelines as applied in the two discovery cohorts. These analyses identified 3,537 significant autosomal eVNTRs that were associated with the expression level of 3,615 unique genes (6,454 pairwise associations) (Table S6) and 3,288 significant autosomal mVNTRs that were associated with methylation levels of 6,999 unique CpGs (9,730 pairwise associations) (Table S7).

When compared to the associations identified in whole blood from the GTEx and PCGC cohorts, we observed replication at genome-wide significance levels and with

concordant directionality for 278 of 381 (73%) GTEx eVNTR:gene pairwise associations and 2,507 of 3,139 (80%) PCGC mVNTR:CpG pairwise associations (Figure 4), yielding strong evidence to support that the majority of associations we report are most likely robust. We also observed a trend for many VNTR loci to be associated with both gene expression and CpG methylation. In the PPMI cohort, of the 3,537 unique eVNTR loci identified, 1,489 (42.1%) were also associated with the methylation level of one or more *cis*-linked CpGs. Of these, 653 (43.9%) had one or more associated CpGs that were located in either the promoter or an annotated enhancer element of the same gene whose expression they associated with. Using GeneHancer annotations, which define promoter and enhancer elements that are linked to the gene(s) they most likely regulate,<sup>43</sup> we identified CpGs that were associated with an mVNTR and lie within annotated promoters or enhancers of eVNTR target genes. We then compared the correlation coefficients between VNTR copy number and both methylation and expression,



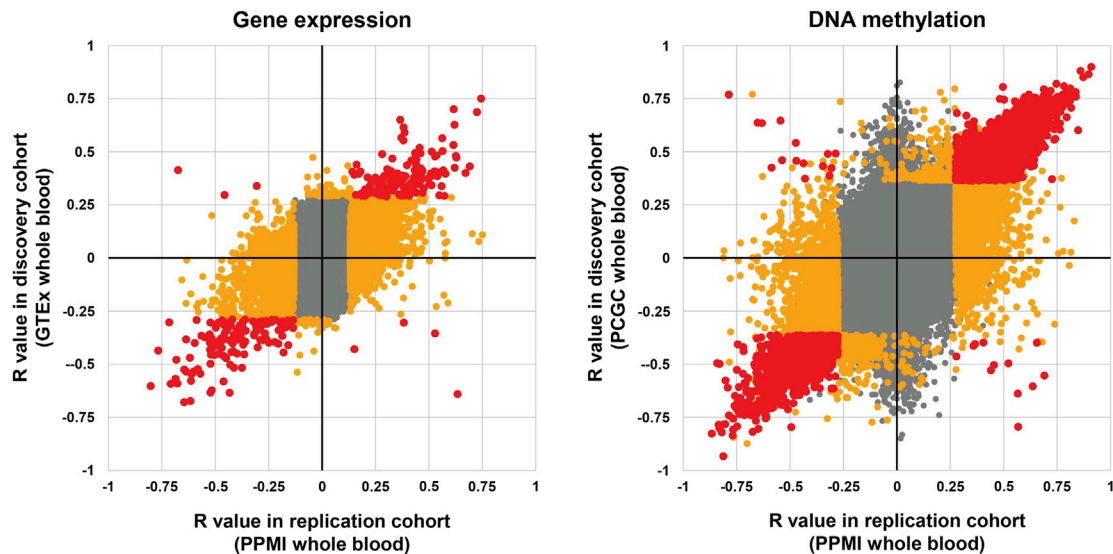


**Figure 4. Replication of the majority of significant eVNTs and mVNTs in an independent cohort**

We performed replication analysis in the PPMI cohort, which comprises 712 individuals, with Illumina WGS, DNA methylation, and RNA-seq data derived from whole blood. We observed that 73% of significant eVNTs detected in GTEx whole blood were also identified as significant in the PPMI cohort. Similarly, 80% of significant mVNTs detected in the PCGC discovery cohort were also significant in the PPMI cohort. Points shown in gray were non-significant in both discovery and replication cohorts, points in orange were significant in one cohort, while points in red were significant in both cohorts.

thereby comparing associations of VNTRs with both gene expression and epigenetics of their annotated regulatory regions. We observed that for both promoters ( $p = 5.8 \times 10^{-10}$ ) and enhancers ( $p = 3.9 \times 10^{-16}$ ), there was a significant inverse relationship between CpG methylation and gene expression, i.e., functional VNTRs preferentially showed opposite directionality of effects on methylation of regulatory elements and expression of the associated genes (Figure S12). This high degree of convergence between these two data types lends further support to our results and suggests that, in at least a subset of cases, the potential mechanism of action of VNTRs on gene expression is via epigenetic modification of regulatory elements.

#### Replication of VNTR:CpG associations via Oxford Nanopore long-read data

We utilized a set of 30 genomes sequenced with Oxford Nanopore technology (ONT) to further validate a subset of mVNTRs. Here, after generating phased genome assemblies,<sup>36</sup> we directly genotyped VNTR copy number on each haplotype by using spanning long reads and determined allelic CpG methylation levels by analysis of electrical current signals from each phased read,<sup>46</sup> allowing direct association of DNA methylation levels with *cis*-linked VNTR alleles (Figure 5A). After quality filtering, data for each VNTR:CpG pair were available for a mean of 24 independent haplotypes and with a mean read depth of 24 $\times$  per CpG on each haplotype.

As a result of the low number of samples, after quality filtering we were only able to assess replication of 228 mVNTR:CpG pairs identified in the PCGC discovery

cohort that had sufficient data for robust analysis because the multiple testing burden for a genome-wide analysis would be prohibitive. We observed a clear trend where the majority of VNTR:CpG associations identified via read depth and Illumina 850k array profiling showed concordant directionality with direct VNTR and methylation measurements from ONT reads, and 163 of 228 (71%) VNTR:CpG pairs showed consistent directionality of association in the two datasets (Figure 5B). It should be noted that given the very small size of this cohort, the relatively coarse resolution of methylation measurements compared with some of the effect sizes, and the different cell type compared with the PCGC discovery cohort, not all loci were expected to show strong replication.

In addition to providing replication for individual CpGs, the use of ONT reads provided much more complete assessment of CpG methylation levels compared with the targeted coverage of the Illumina 850k array, and in several cases, we observed broad clusters of multiple CpGs that showed strong associations with VNTR copy number that were not apparent from array profiling (Figures 5C and 5D). Overall, these data provided additional supporting evidence that read-depth profiling of VNTRs is effective for identifying genuine biological associations.

#### Population stratification and trait associations of VNTRs

We analyzed VNTR copy number in samples from the Human Genome Diversity Panel and used these data to estimate the degree of population stratification in VNTR copy number with the  $V_{ST}$  statistic.<sup>47,48</sup> Examples of VNTRs with high population stratification are shown in Figure 6. We observed strong enrichment for VNTRs with

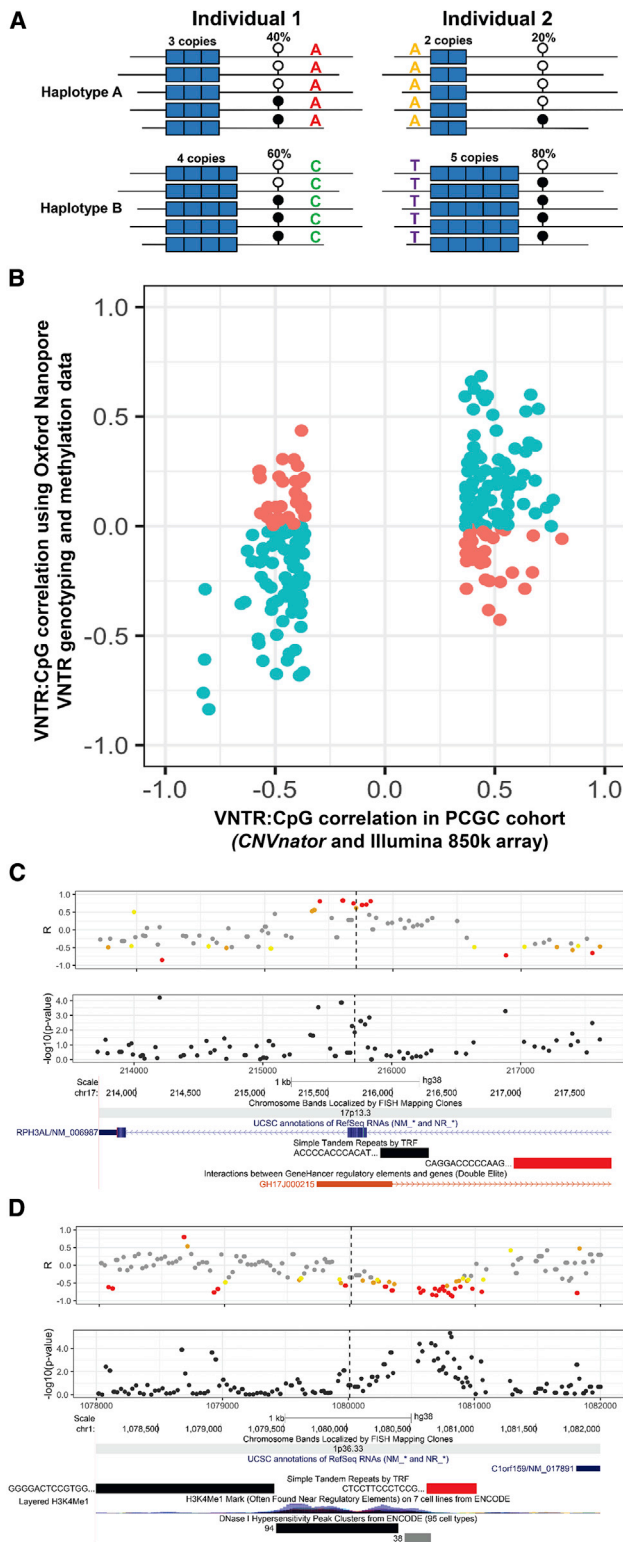


**Figure 5. Additional replication of mVNTRs from direct VNTR genotyping and methylation profiling in 30 genomes sequenced with Oxford Nanopore long reads**

(A) Outline of how phased long reads can be used to perform allelic association analysis of VNTR genotype with *cis*-linked CpG methylation levels. In each individual, ONT reads are phased into the two haplotypes via SNVs (colored letters), VNTRs (blue blocks) are genotyped directly on each haplotype based on the phased assemblies, and CpG methylation levels (lollipops) on

high population divergence within the set of putatively functional VNTRs identified in our discovery cohorts: there were 27 GTEx eVNTRs with  $V_{ST} > 0.2$  (5.7-fold enrichment compared with all VNTR loci tested,  $p = 7.9 \times 10^{-14}$ ) and 120 with  $V_{ST} > 0.1$  (3.8-fold enrichment,  $p = 9.2 \times 10^{-38}$ ), while for mVNTRs in the PCGC cohort, 15 had  $V_{ST} > 0.2$  (6.3-fold enrichment,  $p = 1.3 \times 10^{-8}$ ) and 112 had  $V_{ST} > 0.1$  (6.6-fold enrichment,  $p = 1.5 \times 10^{-57}$ ). We also compared this set of population-stratified VNTRs to TRs that were previously identified as having expanded specifically in the human lineage compared to other primates and observed similar enrichments (GTEx eVNTRs 5.7-fold enriched,  $p = 0.045$ ; PCGC mVNTRs 9.2-fold enriched,  $p = 0.018$ ).<sup>54</sup>

To investigate whether eVNTRs with elevated  $V_{ST}$  levels were enriched for phenotype associations, we annotated eVNTRs with human phenotypes that they potentially regulate by using both the results of PrediXcan and a combination of tissue-matched eQTLs joined with variants from the GWAS Catalog (Table S4). This identified 198 of 2,980 eVNTRs (6.6%) that had trait annotations from PrediXcan, while 634 eVNTRs (21.3%) had annotations derived from the overlap of GWAS Catalog variants and eQTLs. Examples of several functionally interesting candidate eVNTRs that are potentially linked to human traits via annotations from PrediXcan include the following.

- (1) An 87-mer VNTR (chr6: 166,997,608–166,997,912, hg38) that associates with expression of *RNASET2* (MIM: 612944) in esophagus mucosa. *RNASET2* is a secreted extracellular ribonuclease with roles in immune sensing and response and is linked by PrediXcan with risk of Crohn disease, inflammatory bowel disease, and rheumatoid arthritis.<sup>55,56</sup>

each haplotype are estimated on the basis of electrical current signals from each phased read.

(B) For mVNTR:CpG pairs identified in the PCGC discovery cohort that had  $\geq 20$  haplotypes each with  $\geq 10\times$  coverage in the 30 available ONT genomes, 163 of 228 (71%) showed the same directionality of association in this independent dataset.

(C) Copy number of an 83-mer VNTR (chr17: 216,953–218,561, hg38, indicated by the red bar) that lies intronic within *RPH3AL* is positively associated with local DNA methylation, including an annotated enhancer of *RPH3AL*. This same VNTR was negatively associated with *RPH3AL* expression in 22 GTEx tissues.

(D) Copy number of a 32-mer VNTR (chr1: 1,080,637–1,081,029, hg38, indicated by the red bar) that lies  $\sim 800$  bp upstream of *C1orf159* is negatively associated with local DNA methylation, including a region of H3K4 mono-methylation and DNaseI hypersensitivity. This same VNTR was positively associated with *C1orf159* expression in six GTEx tissues. In (C) and (D), plots show the correlation (R) values and unadjusted p values between VNTR copy number and CpG methylation measured directly from ONT reads. The dashed vertical lines indicate the position of a CpG that was associated with VNTR copy number in the PCGC discovery cohort. Correlation values are colored according to their significance in the 30 ONT genomes: yellow indicates  $p < 0.1$ , orange  $p < 0.05$ , and red  $p < 0.01$ . Below the plots are screenshots from the UCSC Genome Browser showing annotations of RefSeq genes, simple repeats, and regulatory regions.

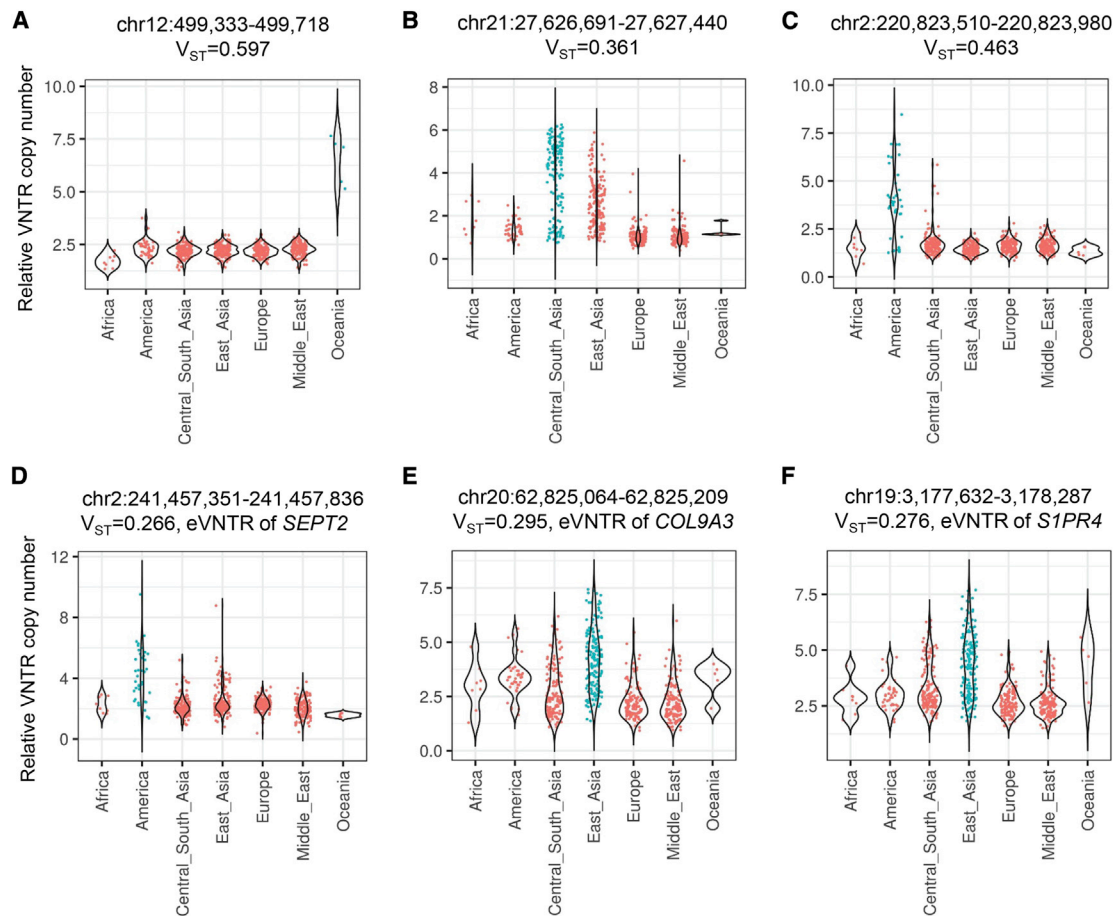


**Figure 6. VNTRs with high population divergence are enriched for functional associations with gene expression, methylation, and human traits**

We estimated population stratification of VNTR copy number with the  $V_{ST}$  statistic in samples from the Human Genome Diversity Panel. Both eVNTRs and mVNTRs were enriched for VNTRs with high  $V_{ST}$ , and consistent with the notion that selection may have acted to modify copy number of functional VNTR loci in specific populations, we also observed that eVNTRs with elevated  $V_{ST}$  were enriched for putative phenotype associations. Shown are six example VNTRs with high  $V_{ST}$ .

- (A) A 40-mer VNTR (chr12: 499,333–499,718, hg38) expanded in the Oceanic population.  
 (B) A 33-mer VNTR (chr21: 27,626,691–27,627,440, hg38) expanded in Asians.  
 (C) A 20-mer VNTR (chr2: 220,823,510–220,823,980, hg38) expanded in Americans.  
 (D) An 81-mer VNTR (chr2: 241,457,351–241,457,836, hg38) expanded in Americans is associated with expression level of *SEPT2* (MIM: 601506) in skin and thyroid and is potentially linked to multiple human traits by GWASs.  
 (E) A 24-mer VNTR (chr20: 62,825,064–62,825,209, hg38) expanded in East Asians is associated with expression level of *COL9A3* (MIM: 120270) in adipose tissue, muscle, and blood.  
 (F) A 39-mer VNTR (chr19: 3,177,632–3,178,287, hg38) expanded in East Asians is associated with expression level of *S1PR4* (MIM: 603751) in mammary tissue, thyroid, and esophagus.

- (2) A VNTR region composed of multiple motifs (chr16: 29,196,863–29,197,354, hg38) that associates with expression of *TUFM* (MIM: 602389) in thyroid. *TUFM* is a mitochondrial elongation factor involved in mitochondrial replication and is linked by PrediXcan with body mass index and hip and waist circumference.<sup>57</sup>  
 (3) A 53-mer VNTR (chr17: 83,032,018–83,032,543, hg38) located intronic within *B3GNTL1* (MIM: 615337) that associates with *B3GNTL1* expression in aorta. *B3GNTL1* is a glycosyltransferase that transfers sugar moieties to acceptor molecules and is linked by PrediXcan with levels of glycosylated hemoglobin.<sup>58</sup>

Consistent with the notion that selection may have acted to modify copy number of functional VNTR loci in specific populations, we observed that eVNTRs with elevated  $V_{ST}$  levels were enriched for putative phenotype associations: 44 GTEx eVNTRs with  $V_{ST} > 0.1$  were linked with GWAS traits, representing a 1.7-fold enrichment when compared with all eVNTRs identified ( $p = 9.0 \times 10^{-5}$ ), while 13 had trait associations from PrediXcan (1.6-fold enrichment,  $p = 0.058$ ).

#### Analysis of eVNTRs and mVNTRs on the X chromosome

In addition to analysis of autosomal loci, we also performed association analysis between VNTR copy number and gene expression and DNA methylation on

the X chromosome. Because of the confounder of X chromosome inactivation, which results in large epigenetic and expression changes over most of the X chromosome in females,<sup>59</sup> we utilized only male samples, resulting in an approximate halving of sample size and a large corresponding reduction in statistical power. We identified 14 eVNTR:gene pairwise associations in the GTEx cohort (Table S8), 12 mVNTR:CpG pairwise associations in the PGC cohort (Table S9), and 36 eVNTR:gene and 36 mVNTR:CpG pairwise associations in the PPMI cohort (Tables S10 and S11).

## Discussion

Here, we have conducted a genome-wide scan for putatively functional VNTRs that associate with local gene expression (eVNTRs) and DNA methylation (mVNTRs) by using two separate cohorts for initial discovery, followed by subsequent replication in a third cohort. In addition, we provided further validation of mVNTRs by using phased genomes sequenced with ONT long reads. We identified thousands of VNTRs where repeat copy number associated with local expression and epigenetics and successfully replicated the majority of these signals at stringent genome-wide significance thresholds. Multiple observations are consistent with a functional role for these loci, including an enrichment for regulatory elements such as gene promoters, annotated enhancer and silencer elements, a strong bias for eVNTRs/mVNTRs to lie in close proximity to their associated gene/CpG, and replication of several known VNTR associations from prior targeted studies. We hypothesize that VNTRs might act to modify gene expression and epigenetics via several different mechanisms. These include modifying the structural properties of the DNA and/or chromatin fiber, changing the number of binding sites for DNA and/or chromatin-associated factors, or altering spacing between regulatory elements and their targets.

Using conditional analysis where we removed the effect of known SNV QTLs for the same gene or CpG that was associated with VNTR copy number, we show that many of the signals we detected are not simply driven by linkage disequilibrium between VNTRs and flanking SNVs. We also investigated stratification of VNTRs by using diverse human populations. As selection resulting from differing environmental pressures represents a potential mechanism leading to high population divergence, elevated  $V_{ST}$  can be an indicator of possible selective effects acting on VNTR copy number. We observed multiple examples of putatively functional eVNTRs and mVNTRs that showed population-specific expansion or contraction. By annotating eVNTRs with possible human traits that they might influence based on the genes they regulate, we found that eVNTRs with elevated  $V_{ST}$  levels were enriched for putative phenotype associations. Finally, we also observed that eVNTRs and mVNTRs were enriched for TRs that have undergone human-specific expansions in copy number.<sup>54</sup>

Overall, these data provide strong evidence to support the notion that copy number variation of some VNTR loci exerts a regulatory effect on the local genome, is most likely associated with a wide variety of human traits and disease susceptibilities, and similar to single nucleotide and other types of structural variation, has most likely been subject to selective pressures during recent evolutionary history.<sup>60–62</sup>

The majority of VNTRs we assayed via read depth were relatively large, exceeding the read length of Illumina WGS (mean motif size 116 bp, mean span of repeat tract in reference genome 353 bp). Because of their size and tandemly repeated nature, copy number variation of VNTRs is difficult to assay in Illumina WGS data via standard tools for genotyping structural variants. By direct comparison with VNTR genotypes derived from long-read sequencing, we observed that CNVnator generally provides relatively good estimates of relative diploid VNTR copy number for the majority of VNTRs in the genome. In contrast, other published tools for genotyping VNTRs are either limited to only being able to genotype alleles that are shorter than the sequencing read length or performed poorly in our hands for the set of VNTRs we assayed.<sup>11,12</sup>

However, the use of read depth does have some major limitations. First, read depth does not provide any allelic information and only yields a relative estimate of total copy number from the sum of both alleles. For example, a heterozygous individual with alleles of two and eight repeats (total  $n = 10$ ) will be indistinguishable from an individual who is homozygous for an allele with five repeats (total  $n = 10$ ). Also, the use of read depth does not differentiate between specific repeat motifs with divergent sequence that may independently vary in copy number, as has been observed to occur at some VNTRs.<sup>4</sup> Furthermore, in the case that a repeat motif strongly diverges from those that are represented in the reference genome, these might be poorly measured or missed entirely because mapping of reads to a VNTR is based on alignment to the reference sequence. We observed some evidence to support this: some VNTRs that showed underestimation of copy number compared with direct genotypes from PacBio WGS often had consistently low read depth within the VNTR locus. Finally, by studying discrepancies between VNTR copy estimates derived from read depth and PacBio WGS, we observed that the accuracy of read depth for genotyping VNTRs is inversely related to both motif size and copy number. Thus, read depth is best suited for studying those VNTRs with larger and higher copy number motifs.

Given that TR loci are frequently misassembled or collapsed during genome assembly, it is therefore likely that our study has not effectively assessed some fraction of VNTRs that are poorly represented in the current reference genome.<sup>52,54,60,63</sup> Ongoing efforts to improve and diversify the human reference genome will most likely provide a more complete ascertainment of VNTRs that are present in the human population.<sup>54,64</sup> The use of read depth to genotype VNTRs can also potentially be confounded

where a VNTR is contained within a larger underlying copy number variation or through batch effects in WGS data. However, here we applied stringent quality control steps to remove such confounders, and through visualization of the underlying data at individual VNTRs and large-scale replication in an independent cohort, we minimized the possibility that these significantly influenced our results.

Other limitations of our analysis are that by using linear regression in our association analysis, we tested a model in which the relationship between expression/DNA methylation and VNTR copy number is presumed to be linear, and therefore, we had limited power to identify more complex non-linear effects of different VNTR alleles that have been observed at some TR loci.<sup>65</sup> Furthermore, we were only able to assay CpG methylation in whole blood, and the measurements of DNA methylation that we used were based on methylation arrays, which only assay a small fraction of all CpGs in the genome. However, using a set of 30 genomes sequenced with ONT long reads, we were able to perform a more complete assessment of methylation levels for a much larger number of CpGs, although here the small size of this cohort and the corresponding lack of statistical power effectively limited us to performing replication analysis of those mVNTR:CpG associations already identified via read depth. Finally, it should be noted that the PCGC and PPMI cohorts are composed of individuals with either congenital heart defects or Parkinson disease, respectively. However, we consider it unlikely that this significantly influences our overall conclusion that variation of some VNTRs is associated with local gene expression and DNA methylation. Overall, despite various technical and biological differences among the cohorts we profiled with Illumina or ONT WGS, we were able to replicate the majority of eVNTRs and mVNTRs, indicating the overall robustness of our results.

Our study provides an initial map of putatively functional VNTRs, and hints that future studies of tandem repeat variation will most likely yield novel insights into the genetic basis of human phenotypes that have been largely ignored in the era of SNV-based GWASs. In order to make results of our association analysis of eVNTRs and mVNTRs easily accessible to the community, we have created new tracks viewable in the UCSC Genome Browser (Figure S13 and [data and code availability](#)). In the future, we postulate that the application of long-read sequencing that provides improved genotyping of VNTRs in large cohorts will lead to deeper insights into the effects of this class of structural variation on diverse human traits.

### Data and code availability

All reported associations of VNTRs with gene expression and DNA methylation are available as Track Hubs within the UCSC Genome Browser, <http://genome.ucsc.edu/cgi-bin/hgHubConnect?hubSearchTerms=VNTR>.

### Supplemental information

Supplemental information can be found online at <https://doi.org/10.1016/j.ajhg.2021.03.016>.

### Declaration of interests

The authors declare no competing interests.

Received: December 16, 2020

Accepted: March 11, 2021

Published: March 31, 2021

### Web resources

1000 Genomes Project high-coverage WGS data, <https://www.internationalgenome.org/data-portal/data-collection/30x-grch38>

Database of Genotypes and Phenotypes (dbGaP) GTEx data, [https://www.ncbi.nlm.nih.gov/projects/gap/cgi-bin/study.cgi?study\\_id=phs000424.v7.p2](https://www.ncbi.nlm.nih.gov/projects/gap/cgi-bin/study.cgi?study_id=phs000424.v7.p2)

Database of Genotypes and Phenotypes (dbGaP) PCGC data, [https://www.ncbi.nlm.nih.gov/projects/gap/cgi-bin/study.cgi?study\\_id=phs001138.v1.p2](https://www.ncbi.nlm.nih.gov/projects/gap/cgi-bin/study.cgi?study_id=phs001138.v1.p2)

Gene Expression Omnibus (GEO) PCGC data, <https://www.ncbi.nlm.nih.gov/geo/query/acc.cgi?acc=GSE159930>

GTEx portal, <https://www.gtexportal.org/>

GWAS catalog, <https://www.ebi.ac.uk/gwas/>

Human Genome Diversity Panel, <https://www.internationalgenome.org/data-portal/data-collection/hgdp>

Human Pangenome Reference Consortium, <https://github.com/human-pangenomics/hpgp-data>

OMIM, <http://www.omim.org/>

Parkinson's Progression Markers Initiative (PPMI), <https://www.ppmi-info.org/>

The International Genome Sample Resource, <https://www.internationalgenome.org/data-portal/data-collection/30x-grch38>

UCSC Genome Browser, <http://genome.ucsc.edu>

### References

1. Lander, E.S., Linton, L.M., Birren, B., Nusbaum, C., Zody, M.C., Baldwin, J., Devon, K., Dewar, K., Doyle, M., FitzHugh, W., et al.; International Human Genome Sequencing Consortium (2001). Initial sequencing and analysis of the human genome. *Nature* 409, 860–921.
2. Perry, G.H., Dominy, N.J., Claw, K.G., Lee, A.S., Fiegler, H., Redon, R., Werner, J., Villanea, F.A., Mountain, J.L., Misra, R., et al. (2007). Diet and the evolution of human amylase gene copy number variation. *Nat. Genet.* 39, 1256–1260.
3. Warburton, P.E., Hasson, D., Guillem, F., Lescale, C., Jin, X., and Abrusan, G. (2008). Analysis of the largest tandemly repeated DNA families in the human genome. *BMC Genomics* 9, 533.
4. Course, M.M., Gudsnuk, K., Smukowski, S.N., Winston, K., Desai, N., Ross, J.P., Sulovari, A., Bourassa, C.V., Spiegelman, D., Couthouis, J., et al. (2020). Evolution of a Human-Specific

- Tandem Repeat Associated with ALS. *Am. J. Hum. Genet.* *107*, 445–460.
5. Song, J.H.T., Lowe, C.B., and Kingsley, D.M. (2018). Characterization of a Human-Specific Tandem Repeat Associated with Bipolar Disorder and Schizophrenia. *Am. J. Hum. Genet.* *103*, 421–430.
  6. Chaisson, M.J.P., Sanders, A.D., Zhao, X., Malhotra, A., Porubsky, D., Rausch, T., Gardner, E.J., Rodriguez, O.L., Guo, L., Collins, R.L., et al. (2019). Multi-platform discovery of haplotype-resolved structural variation in human genomes. *Nat. Commun.* *10*, 1784.
  7. Dashnow, H., Lek, M., Phipson, B., Halman, A., Sadedin, S., Lonsdale, A., Davis, M., Lamont, P., Clayton, J.S., Laing, N.G., et al. (2018). STRetch: detecting and discovering pathogenic short tandem repeat expansions. *Genome Biol.* *19*, 121.
  8. Mousavi, N., Shleizer-Burko, S., Yanicky, R., and Gymrek, M. (2019). Profiling the genome-wide landscape of tandem repeat expansions. *Nucleic Acids Res.* *47*, e90.
  9. Dolzhenko, E., van Vugt, J.J.F.A., Shaw, R.J., Bekritsky, M.A., van Blitterswijk, M., Narzisi, G., Ajay, S.S., Rajan, V., Lajoie, B.R., Johnson, N.H., et al.; US–Venezuela Collaborative Research Group (2017). Detection of long repeat expansions from PCR-free whole-genome sequence data. *Genome Res.* *27*, 1895–1903.
  10. Willems, T., Zielinski, D., Yuan, J., Gordon, A., Gymrek, M., and Erlich, Y. (2017). Genome-wide profiling of heritable and de novo STR variations. *Nat. Methods* *14*, 590–592.
  11. Bakhtiari, M., Shleizer-Burko, S., Gymrek, M., Bansal, V., and Bafna, V. (2018). Targeted genotyping of variable number tandem repeats with adVNTR. *Genome Res.* *28*, 1709–1719.
  12. Gelfand, Y., Hernandez, Y., Loving, J., and Benson, G. (2014). VNTRseek—a computational tool to detect tandem repeat variants in high-throughput sequencing data. *Nucleic Acids Res.* *42*, 8884–8894.
  13. Quilez, J., Guilmatre, A., Garg, P., Highnam, G., Gymrek, M., Erlich, Y., Joshi, R.S., Mittelman, D., and Sharp, A.J. (2016). Polymorphic tandem repeats within gene promoters act as modifiers of gene expression and DNA methylation in humans. *Nucleic Acids Res.* *44*, 3750–3762.
  14. Gymrek, M., Willems, T., Guilmatre, A., Zeng, H., Markus, B., Georgiev, S., Daly, M.J., Price, A.L., Pritchard, J.K., Sharp, A.J., and Erlich, Y. (2016). Abundant contribution of short tandem repeats to gene expression variation in humans. *Nat. Genet.* *48*, 22–29.
  15. Fotsing, S.F., Margoliash, J., Wang, C., Saini, S., Yanicky, R., Shleizer-Burko, S., Goren, A., and Gymrek, M. (2019). The impact of short tandem repeat variation on gene expression. *Nat. Genet.* *51*, 1652–1659.
  16. Brahmachary, M., Guilmatre, A., Quilez, J., Hasson, D., Borel, C., Warburton, P., and Sharp, A.J. (2014). Digital genotyping of macrosatellites and multicopy genes reveals novel biological functions associated with copy number variation of large tandem repeats. *PLoS Genet.* *10*, e1004418.
  17. Borel, C., Migliavacca, E., Letourneau, A., Gagnebin, M., Béna, F., Sailani, M.R., Dermizakis, E.T., Sharp, A.J., and Antonarakis, S.E. (2012). Tandem repeat sequence variation as causative cis-eQTLs for protein-coding gene expression variation: the case of CSTB. *Hum. Mutat.* *33*, 1302–1309.
  18. Deckert, J., Catalano, M., Syagailo, Y.V., Bosi, M., Okladnova, O., Di Bella, D., Nöthen, M.M., Maffei, P., Franke, P., Fritze, J., et al. (1999). Excess of high activity monoamine oxidase A gene promoter alleles in female patients with panic disorder. *Hum. Mol. Genet.* *8*, 621–624.
  19. Guo, G., Ou, X.M., Roettger, M., and Shih, J.C. (2008). The VNTR 2 repeat in MAOA and delinquent behavior in adolescence and young adulthood: associations and MAOA promoter activity. *Eur. J. Hum. Genet.* *16*, 626–634.
  20. Rodríguez, S., Gaunt, T.R., O’Dell, S.D., Chen, X.H., Gu, D., Hawe, E., Miller, G.J., Humphries, S.E., and Day, I.N.M. (2004). Haplotypic analyses of the IGF2-INS-TH gene cluster in relation to cardiovascular risk traits. *Hum. Mol. Genet.* *13*, 715–725.
  21. Santoro, N., Cirillo, G., Amato, A., Luongo, C., Raimondo, P., D’Aniello, A., Perrone, L., and Miraglia del Giudice, E. (2006). Insulin gene variable number of tandem repeats (INS VNTR) genotype and metabolic syndrome in childhood obesity. *J. Clin. Endocrinol. Metab.* *91*, 4641–4644.
  22. De Roeck, A., Duchateau, L., Van Dongen, J., Cacace, R., Bjerke, M., Van den Bossche, T., Cras, P., Vandenberghe, R., De Deyn, P.P., Engelborghs, S., et al.; BELNEU Consortium (2018). An intronic VNTR affects splicing of ABCA7 and increases risk of Alzheimer’s disease. *Acta Neuropathol.* *135*, 827–837.
  23. Manolio, T.A., Collins, F.S., Cox, N.J., Goldstein, D.B., Hindorf, L.A., Hunter, D.J., McCarthy, M.I., Ramos, E.M., Cardon, L.R., Chakravarti, A., et al. (2009). Finding the missing heritability of complex diseases. *Nature* *461*, 747–753.
  24. Eichler, E.E., Flint, J., Gibson, G., Kong, A., Leal, S.M., Moore, J.H., and Nadeau, J.H. (2010). Missing heritability and strategies for finding the underlying causes of complex disease. *Nat. Rev. Genet.* *11*, 446–450.
  25. Gelb, B., Brueckner, M., Chung, W., Goldmuntz, E., Kaltman, J., Kaski, J.P., Kim, R., Kline, J., Mercer-Rosa, L., Porter, G., et al.; Pediatric Cardiac Genomics Consortium (2013). The congenital heart disease genetic network study: Rationale, design, and early results. *Circ. Res.* *112*, 698–706.
  26. Hoang, T.T., Goldmuntz, E., Roberts, A.E., Chung, W.K., Kline, J.K., Deanfield, J.E., Giardini, A., Aleman, A., Gelb, B.D., Mac Neal, M., et al. (2018). The congenital heart disease genetic network study: Cohort description. *PLoS ONE* *13*, e0191319.
  27. Martin-Trujillo, A., Patel, N., Richter, F., Jadhav, B., Garg, P., Morton, S.U., McKean, D.M., DePalma, S.R., Goldmuntz, E., Gruber, D., et al. (2020). Rare genetic variation at transcription factor binding sites modulates local DNA methylation profiles. *PLoS Genet.* *16*, e1009189.
  28. Marek, K., Chowdhury, S., Siderowf, A., Lasch, S., Coffey, C.S., Caspell-Garcia, C., Simuni, T., Jennings, D., Tanner, C.M., Trojanowski, J.Q., et al.; Parkinson’s Progression Markers Initiative (2018). The Parkinson’s progression markers initiative (PPMI) - establishing a PD biomarker cohort. *Ann. Clin. Transl. Neurol.* *5*, 1460–1477.
  29. Abyzov, A., Urban, A.E., Snyder, M., and Gerstein, M. (2011). CNVnator: an approach to discover, genotype, and characterize typical and atypical CNVs from family and population genome sequencing. *Genome Res.* *21*, 974–984.
  30. Näslund, K., Saetre, P., von Salomé, J., Bergström, T.F., Jareborg, N., and Jazin, E. (2005). Genome-wide prediction of human VNTRs. *Genomics* *85*, 24–35.
  31. Audano, P.A., Sulovari, A., Graves-Lindsay, T.A., Cantsilieris, S., Sorensen, M., Welch, A.E., Dougherty, M.L., Nelson, B.J., Shah, A., Dutcher, S.K., et al. (2019). Characterizing the Major Structural Variant Alleles of the Human Genome. *Cell* *176*, 663–675.e19.

32. Stranger, B.E., Nica, A.C., Forrest, M.S., Dimas, A., Bird, C.P., Beazley, C., Ingle, C.E., Dunning, M., Flicek, P., Koller, D., et al. (2007). Population genomics of human gene expression. *Nat. Genet.* 39, 1217–1224.
33. Gibbs, J.R., van der Brug, M.P., Hernandez, D.G., Traynor, B.J., Nalls, M.A., Lai, S.L., Arepalli, S., Dillman, A., Rafferty, I.P., Troncoso, J., et al. (2010). Abundant quantitative trait loci exist for DNA methylation and gene expression in human brain. *PLoS Genet.* 6, e1000952.
34. Conrad, D.F., Pinto, D., Redon, R., Feuk, L., Gokcumen, O., Zhang, Y., Aerts, J., Andrews, T.D., Barnes, C., Campbell, P., et al.; Wellcome Trust Case Control Consortium (2010). Origins and functional impact of copy number variation in the human genome. *Nature* 464, 704–712.
35. McCaw, Z.R., Lane, J.M., Saxena, R., Redline, S., and Lin, X. (2020). Operating characteristics of the rank-based inverse normal transformation for quantitative trait analysis in genome-wide association studies. *Biometrics* 76, 1262–1272.
36. Rodriguez, O.L., Ritz, A., Sharp, A.J., and Bashir, A. (2020). MsPAC: a tool for haplotype-phased structural variant detection. *Bioinformatics* 36, 922–924.
37. Patterson, M., Marschall, T., Pisanti, N., van Iersel, L., Stougie, L., Klau, G.W., and Schönhuth, A. (2015). WhatsHap: Weighted Haplotype Assembly for Future-Generation Sequencing Reads. *J. Comput. Biol.* 22, 498–509.
38. Ummat, A., and Bashir, A. (2014). Resolving complex tandem repeats with long reads. *Bioinformatics* 30, 3491–3498.
39. Stegle, O., Parts, L., Piipari, M., Winn, J., and Durbin, R. (2012). Using probabilistic estimation of expression residuals (PEER) to obtain increased power and interpretability of gene expression analyses. *Nat. Protoc.* 7, 500–507.
40. Benjamini, Y., and Hochberg, Y. (1995). Controlling the False Discovery Rate: A Practical and Powerful Approach to Multiple Testing. *J. R. Stat. Soc. B* 57, 289–300.
41. Pedersen, B.S., and Quinlan, A.R. (2017). Who's Who? Detecting and Resolving Sample Anomalies in Human DNA Sequencing Studies with Peddy. *Am. J. Hum. Genet.* 100, 406–413.
42. Houseman, E.A., Accomando, W.P., Koestler, D.C., Christensen, B.C., Marsit, C.J., Nelson, H.H., Wiencke, J.K., and Kelsey, K.T. (2012). DNA methylation arrays as surrogate measures of cell mixture distribution. *BMC Bioinformatics* 13, 86.
43. Fishilevich, S., Nudel, R., Rappaport, N., Hadar, R., Plaschkes, I., Iny Stein, T., Rosen, N., Kohn, A., Twik, M., Safran, M., et al. (2017). GeneHancer: genome-wide integration of enhancers and target genes in GeneCards. *Database (Oxford)* 2017, bax028.
44. Pang, B., and Snyder, M.P. (2020). Systematic identification of silencers in human cells. *Nat. Genet.* 52, 254–263.
45. Li, H. (2018). Minimap2: pairwise alignment for nucleotide sequences. *Bioinformatics* 34, 3094–3100.
46. Simpson, J.T., Workman, R.E., Zuzarte, P.C., David, M., Dursi, L.J., and Timp, W. (2017). Detecting DNA cytosine methylation using nanopore sequencing. *Nat. Methods* 14, 407–410.
47. Bergström, A., McCarthy, S.A., Hui, R., Almarri, M.A., Ayub, Q., Danecek, P., Chen, Y., Felkel, S., Hallast, P., Kamm, J., et al. (2020). Insights into human genetic variation and population history from 929 diverse genomes. *Science* 367, eaay5012.
48. Redon, R., Ishikawa, S., Fitch, K.R., Feuk, L., Perry, G.H., Andrews, T.D., Fiegler, H., Shapero, M.H., Carson, A.R., Chen, W., et al. (2006). Global variation in copy number in the human genome. *Nature* 444, 444–454.
49. Barbeira, A.N., Dickinson, S.P., Bonazzola, R., Zheng, J., Wheeler, H.E., Torres, J.M., Torstenson, E.S., Shah, K.P., Garcia, T., Edwards, T.L., et al.; GTEx Consortium (2018). Exploring the phenotypic consequences of tissue specific gene expression variation inferred from GWAS summary statistics. *Nat. Commun.* 9, 1825.
50. Battle, A., Brown, C.D., Engelhardt, B.E., Montgomery, S.B., et al.; GTEx Consortium; Laboratory, Data Analysis & Coordinating Center (LDACC)—Analysis Working Group; Statistical Methods groups—Analysis Working Group; Enhancing GTEx (eGTEx) groups; NIH Common Fund; NIH/NCI (2017). Genetic effects on gene expression across human tissues. *Nature* 550, 204–213.
51. Li, M., Jaffe, A.E., Straub, R.E., Tao, R., Shin, J.H., Wang, Y., Chen, Q., Li, C., Jia, Y., Ohi, K., et al. (2016). A human-specific AS3MT isoform and BORCS7 are molecular risk factors in the 10q24.32 schizophrenia-associated locus. *Nat. Med.* 22, 649–656.
52. Bellizzi, D., Covello, G., Di Cianni, F., Tong, Q., and De Benedictis, G. (2009). Identification of GATA2 and AP-1 Activator elements within the enhancer VNTR occurring in intron 5 of the human SIRT3 gene. *Mol. Cells* 28, 87–92.
53. Örd, T., Puurand, T., Örd, D., Annilo, T., Möls, M., Remm, M., and Örd, T. (2020). A human-specific VNTR in the TRIB3 promoter causes gene expression variation between individuals. *PLoS Genet.* 16, e1008981.
54. Sulovari, A., Li, R., Audano, P.A., Porubsky, D., Vollger, M.R., Logsdon, G.A., Warren, W.C., Pollen, A.A., Chaisson, M.J.P., Eichler, E.E.; and Human Genome Structural Variation Consortium (2019). Human-specific tandem repeat expansion and differential gene expression during primate evolution. *Proc. Natl. Acad. Sci. USA* 116, 23243–23253.
55. Scaldaferrri, D., Bosi, A., Fabbri, M., Pedrini, E., Inforzato, A., Valli, R., Frattini, A., De Vito, A., Noonan, D.M., Taramelli, R., et al. (2018). The human RNASET2 protein affects the polarization pattern of human macrophages in vitro. *Immunol. Lett.* 203, 102–111.
56. Ostendorf, T., Zillinger, T., Andryka, K., Schlee-Guimaraes, T.M., Schmitz, S., Marx, S., Bayrak, K., Linke, R., Salgert, S., Wegner, J., et al. (2020). Immune Sensing of Synthetic, Bacterial, and Protozoan RNA by Toll-like Receptor 8 Requires Coordinated Processing by RNase T2 and RNase 2. *Immunity* 52, 591–605.e6.
57. Bogenhagen, D.F., Rousseau, D., and Burke, S. (2008). The layered structure of human mitochondrial DNA nucleoids. *J. Biol. Chem.* 283, 3665–3675.
58. Zheng, H., Li, Y., Ji, C., Li, J., Zhang, J., Yin, G., Xu, J., Ye, X., Wu, M., Zou, X., et al. (2004). Characterization of a cDNA encoding a protein with limited similarity to  $\beta$ 1, 3-N-acetylglucosaminyltransferase. *Mol. Biol. Rep.* 31, 171–175.
59. Galupa, R., and Heard, E. (2018). X-Chromosome Inactivation: A Crossroads Between Chromosome Architecture and Gene Regulation. *Annu. Rev. Genet.* 52, 535–566.
60. Sabeti, P.C., Varilly, P., Fry, B., Lohmueller, J., Hostetter, E., Cotsapas, C., Xie, X., Byrne, E.H., McCarroll, S.A., Gaudet, R., et al.; International HapMap Consortium (2007). Genome-wide detection and characterization of positive selection in human populations. *Nature* 449, 913–918.
61. Pickrell, J.K., Coop, G., Novembre, J., Kudaravalli, S., Li, J.Z., Absher, D., Srinivasan, B.S., Barsh, G.S., Myers, R.M., Feldman,

- M.W., and Pritchard, J.K. (2009). Signals of recent positive selection in a worldwide sample of human populations. *Genome Res.* *19*, 826–837.
62. Almarri, M.A., Bergström, A., Prado-Martinez, J., Yang, F., Fu, B., Dunham, A.S., Chen, Y., Hurles, M.E., Tyler-Smith, C., and Xue, Y. (2020). Population Structure, Stratification, and Introgression of Human Structural Variation. *Cell* *182*, 189–199.e15.
63. Tørresen, O.K., Star, B., Mier, P., Andrade-Navarro, M.A., Bateman, A., Jarnot, P., Gruca, A., Grynberg, M., Kajava, A.V., Promponas, V.J., et al. (2019). Tandem repeats lead to sequence assembly errors and impose multi-level challenges for genome and protein databases. *Nucleic Acids Res.* *47*, 10994–11006.
64. Miga, K.H., Koren, S., Rhie, A., Vollger, M.R., Gershman, A., Bzikadze, A., Brooks, S., Howe, E., Porubsky, D., Logsdon, G.A., et al. (2020). Telomere-to-telomere assembly of a complete human X chromosome. *Nature* *585*, 79–84.
65. Vences, M.D., Legendre, M., Caldara, M., Hagihara, M., and Verstrepen, K.J. (2009). Unstable tandem repeats in promoters confer transcriptional evolvability. *Science* *324*, 1213–1216.



**The American Journal of Human Genetics, Volume 108**

**Supplemental information**

**Pervasive *cis* effects of variation in  
copy number of large tandem repeats  
on local DNA methylation and gene expression**

**Paras Garg, Alejandro Martin-Trujillo, Oscar L. Rodriguez, Scott J. Gies, Elina Hadelia, Bharati Jadhav, Miten Jain, Benedict Paten, and Andrew J. Sharp**

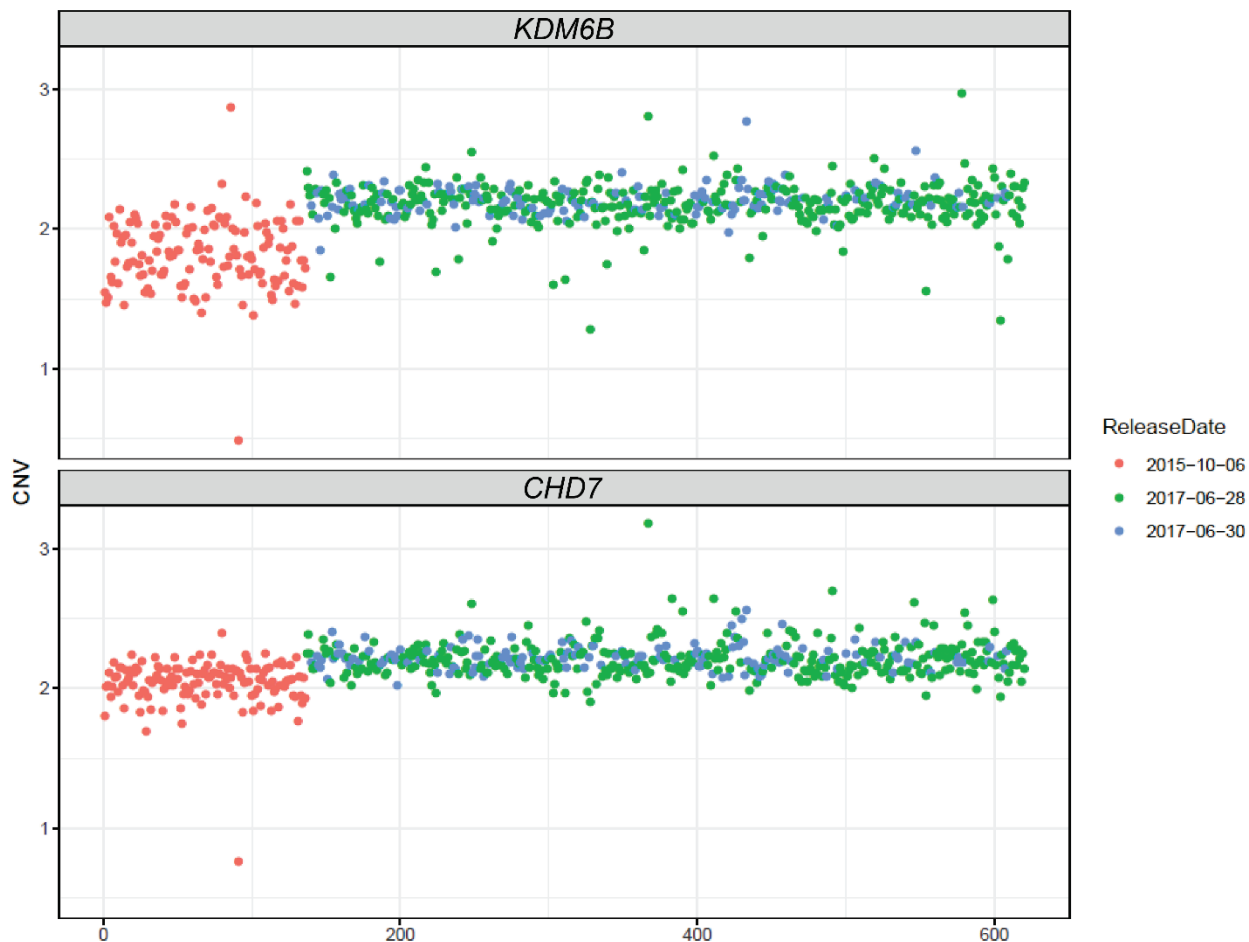


**Figure S1. Batch effects in *CNVnator* copy number estimates from WGS in the GTEx cohort.** Using *CNVnator* data for two highly constrained genes that should remain copy-number invariant in the normal population (*KDM6B* [MIM: 611577], chr17:7,839,904-7,854,796 and *CHD7* [MIM: 608892], chr8:60,678,740-60,868,028, hg38), we observed a strong batch effect in the GTEx cohort, whereby copy numbers derived from WGS data with release date October 6<sup>th</sup> 2015 (*red points*) were systematically shifted compared to later data releases (*blue and green points*). Based on these observations, we removed from further analysis all 135 samples with release October 6th 2015.

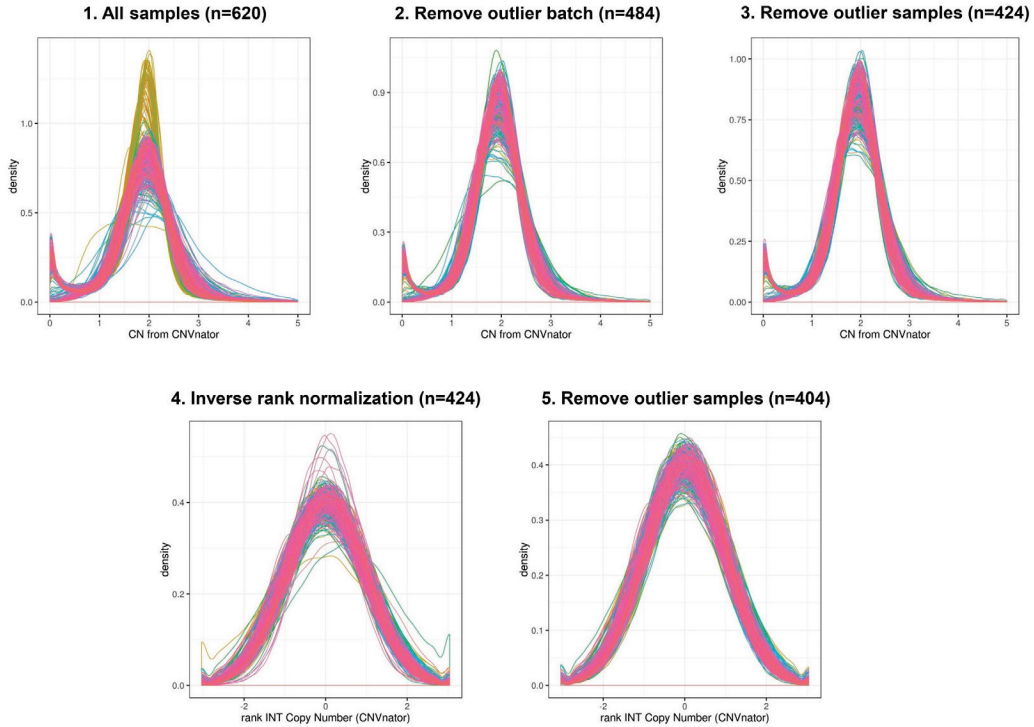


**Figure S2. VNTR copy number distributions within the GTEx cohort after sample filtering and data normalization.** Based on *CNVnator* copy number estimates of 89,893 autosomal - VNTRs, we generated density plots at each step of quality control and normalization. We initially analyzed WGS data from 620 individuals, but after removal of batch effects, samples that were consistent outliers at invariant constrained genomic loci, or outliers for VNTR copy number by principal component analysis and density plots, we used a final cohort of 404 samples in our analysis.

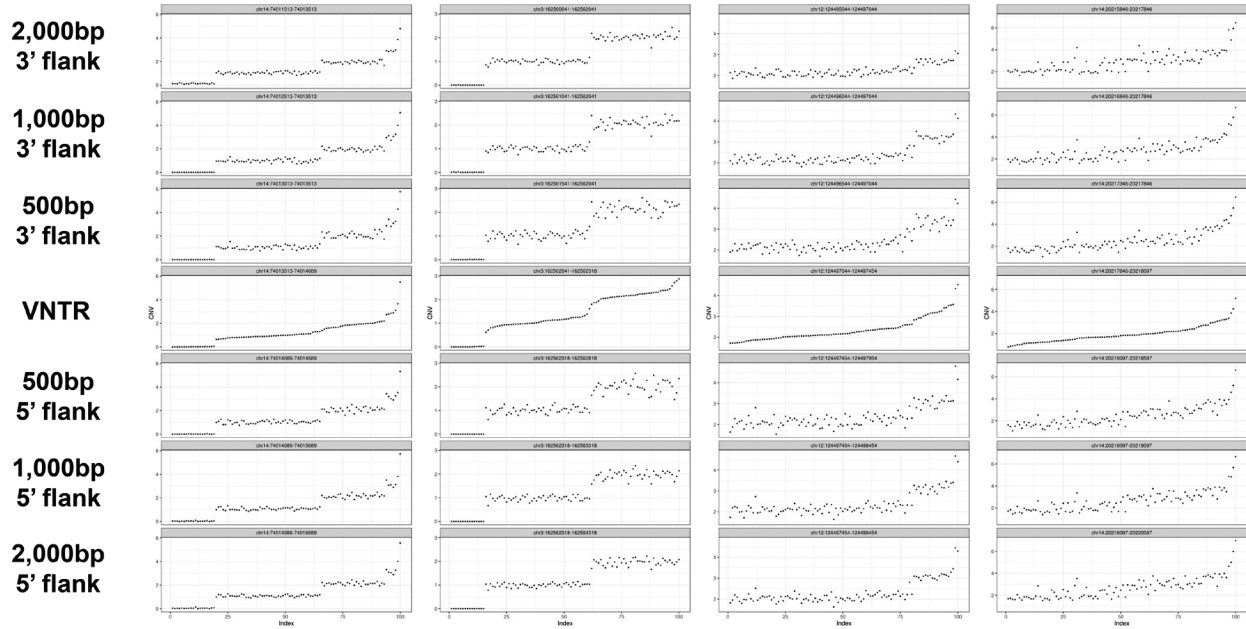


**Figure S3. VNTR copy number estimates using *CNVnator* can be confounded by the presence of larger underlying CNVs.** In situations where a VNTR is embedded within a larger copy number variable region, copy number estimates for the VNTR based on *CNVnator* read depth can be influenced by underlying variations of the wider region. To identify VNTRs that were subject to this confounder, we analyzed the 3' and 5' 500bp, 1kb and 2kb regions flanking each VNTR using *CNVnator*, and then correlated the values of the 1kb flanks with VNTR copy number. Shown are data from four representative loci that were removed from further analysis. Within each locus, samples are ordered based on the estimated VNTR copy number, revealing that the observed estimates of VNTR copy number are highly correlated with variation in the flanking regions, and likely simply reflect a larger underlying CNV, rather than changes in length of the VNTR array itself.

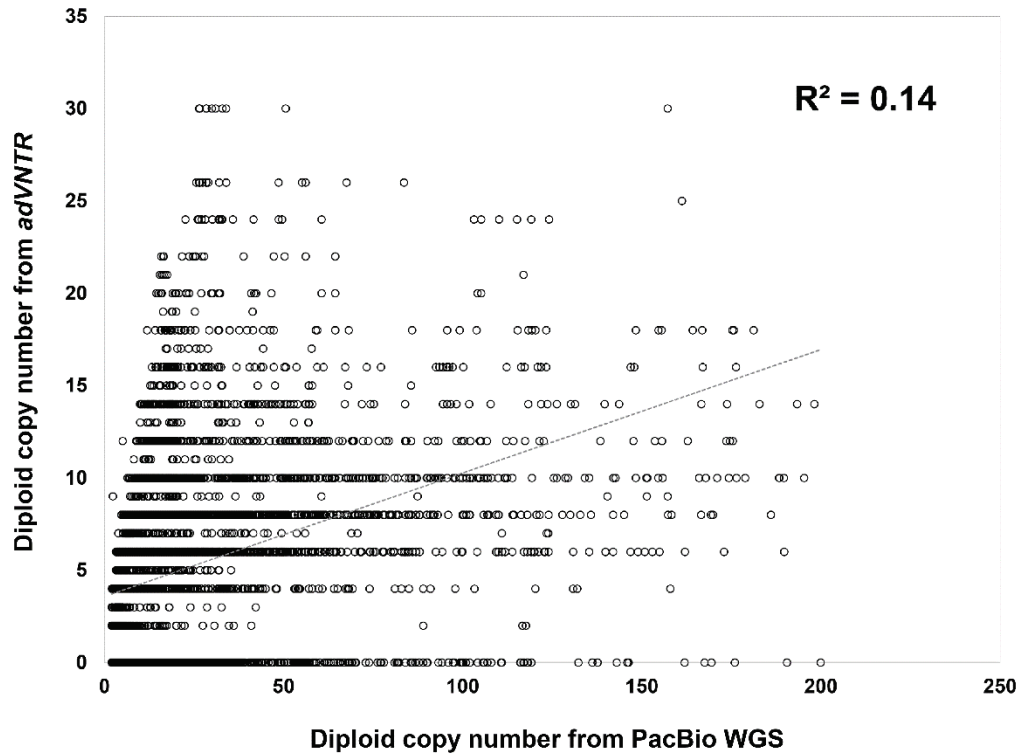


**Figure S4. Poor performance of *adVNTR* for genotyping VNTRs.** Using data for the same set of 1,891 VNTRs in 14 individuals as shown in Figure 1B (see Methods), we used *adVNTR* to generate VNTR genotypes. When compared with direct genotypes generated from PacBio long-read WGS in these same individuals, we observed an  $R^2=0.14$ , indicating generally poor accuracy of this tool when applied to this set of VNTRs (Table S3).

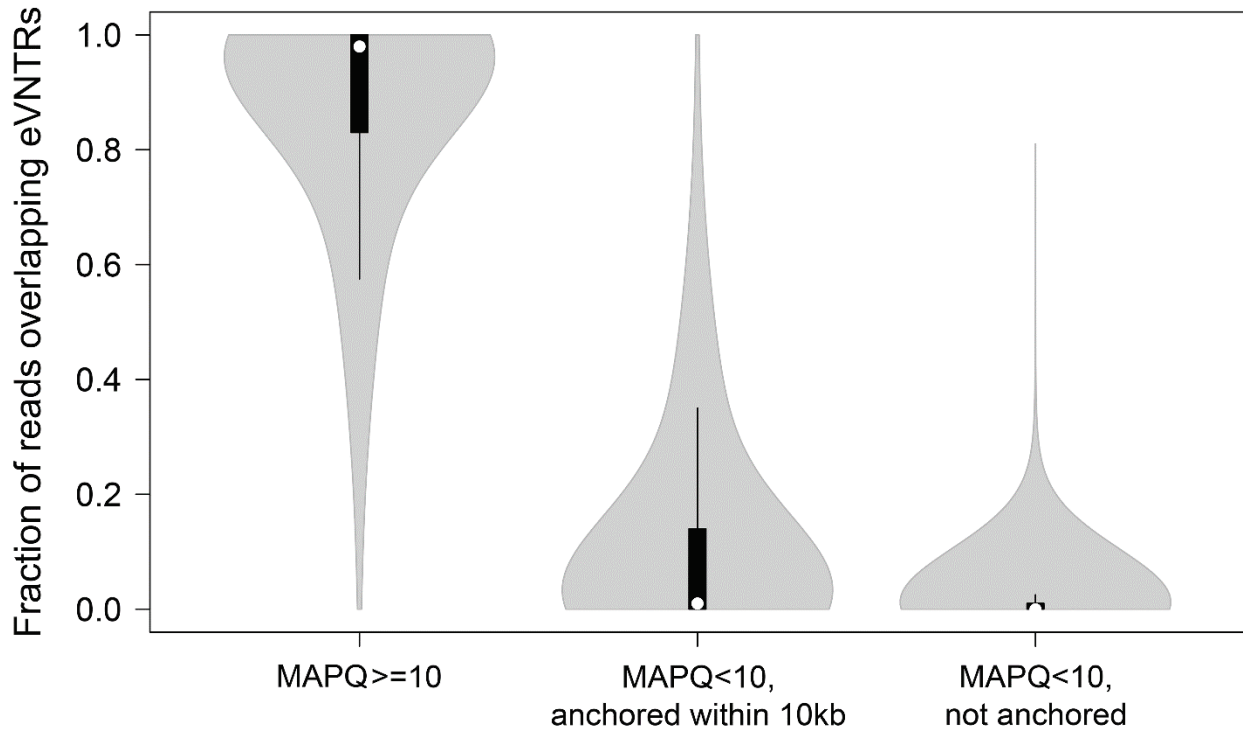


**Figure S5. Assessment of the reliability of Illumina reads mapping to VNTR loci.** We analyzed Illumina reads mapping to 2,980 autosomal GTEx eVNTRs in a Yoruban sample (NA18874), classifying them into three categories: (i)  $\text{MAPQ} \geq 10$ , (ii)  $\text{MAPQ} < 10$ , but with a mate-pair that mapped reliably within  $\pm 10\text{kb}$ . (iii)  $\text{MAPQ} < 10$ , without a mate pair that was anchored within  $\pm 10\text{kb}$ . Violin plots show the fraction of reads in each of these three categories at each eVNTR locus. Overall, copy number estimates for the vast majority of eVNTRs were based on reliably mapped reads, with only a single eVNTR containing  $>50\%$  of unreliably mapped reads. Within each violin, the median is indicated by the white dot, box limits indicate the 25<sup>th</sup> and 75<sup>th</sup> percentiles, and whiskers extend 1.5 times the interquartile range from the 25<sup>th</sup> and 75<sup>th</sup> percentiles.

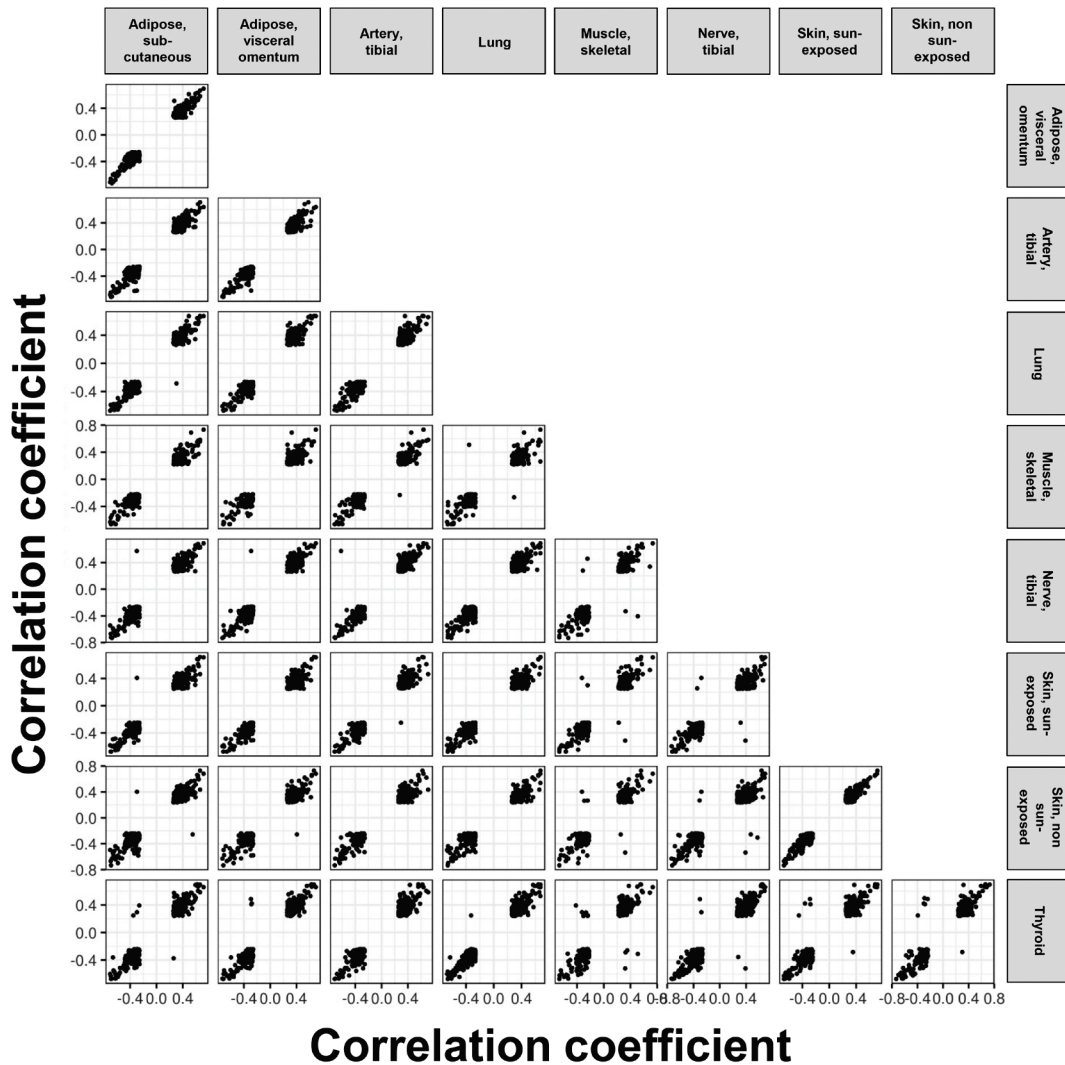


**Figure S6. Pairwise correlation patterns of significant eVNTR:gene associations across eight tissues.** Each point shows the R values of an individual gene:eVNTR pair that was significant in both tissues. In nearly all cases, the directionality of the observed associations are concordant among different tissues, with only 0.6% of eVNTR:gene pairs showing opposite direction of effect in different tissues, consistent with our results representing genuine associations.

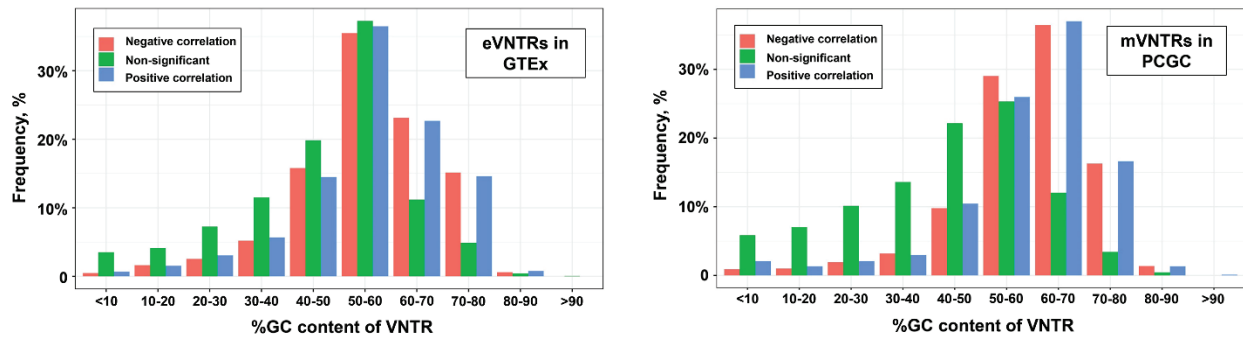


**Figure S7. Significant eVNTRs and mVNTRs are biased towards higher GC content.** We observed that both putatively functional eVNTRs and mVNTRs showed a clear trend to be composed of motifs with higher GC-content than the background of all VNTRs tested. This trend was stronger for mVNTRs, which is consistent with the Illumina 850k array preferentially sampling CpG in GC-rich regions of the genome, and the observation that most mVNTRs are located physically close (<5kb) from the CpGs that they associated with.



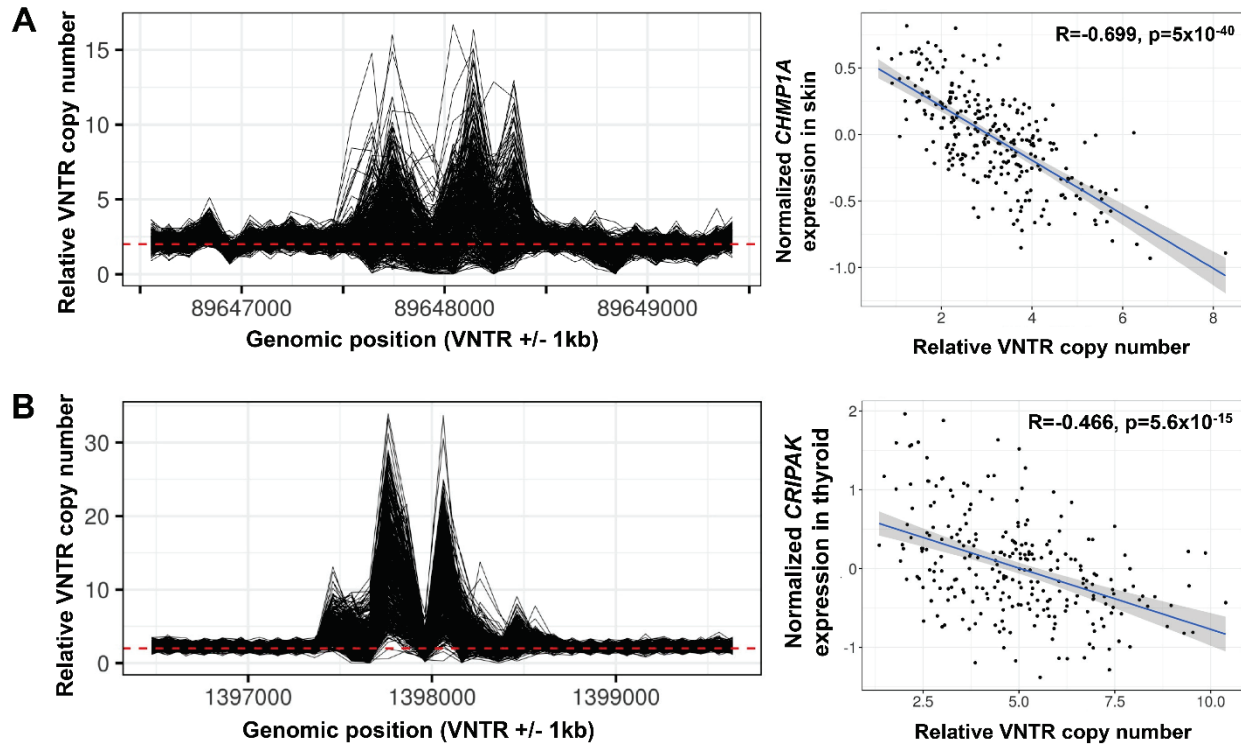


**Figure S8. Two example eVNTR loci detected in the GTEx cohort. (A)** A 42mer repeat (chr16:89,647,518-89,648,445, hg38) located intronic within *CHMP1A* [MIM: 164010] associates negatively with *CHMP1A* expression in multiple tissues (shown is data from skin, sun exposed lower leg). **(B)** A 45mer repeat (chr4:1,397,437-1,398,660, hg38) located 1.4 kb downstream of *CRIPAK* [MIM: 610203] associates negatively with *CRIPAK* expression in multiple tissues (shown is expression data from thyroid). *CNVnator* locus plots show estimated copy number per 100bp bin over the VNTR region, extending 1kb each side, with the red dashed line indicating diploid copy number equal to that of the reference genome.

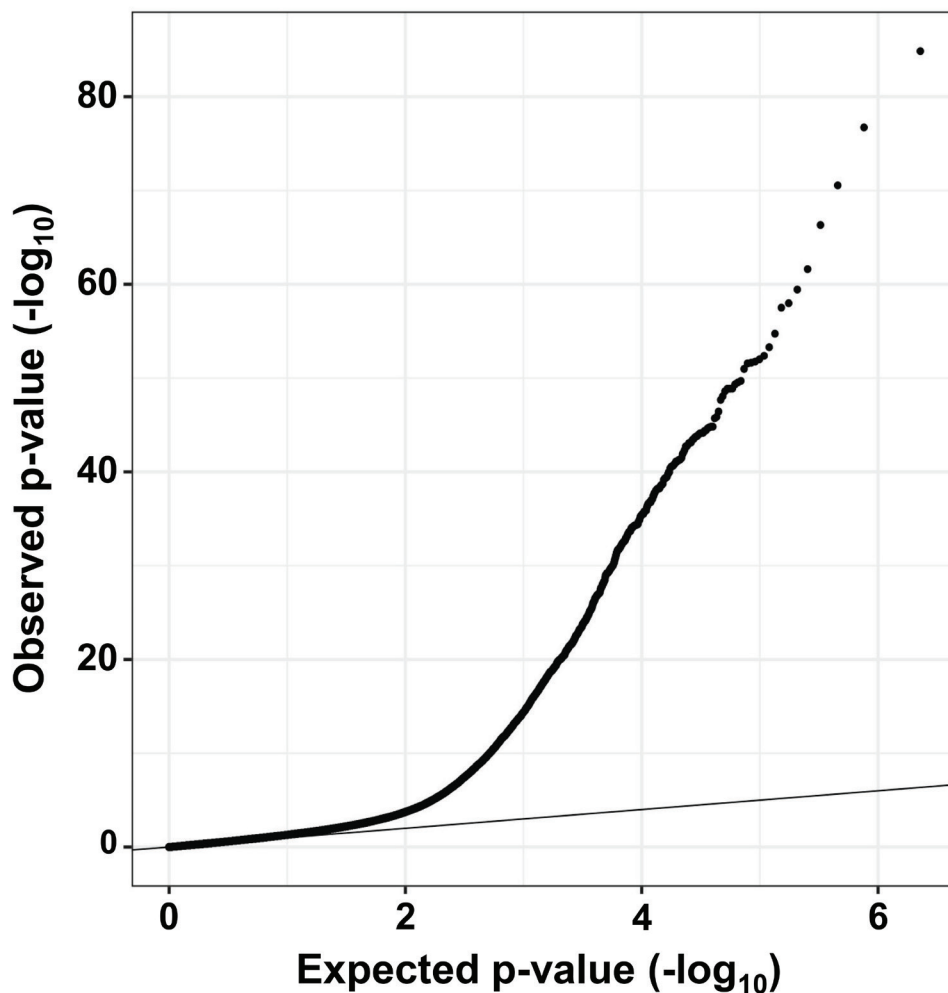


**Figure S9. QQ plot showing the distribution of observed versus expected p-values for mVNTRs in whole blood from the PCGC.** In this cohort we observed some evidence for genomic inflation ( $\lambda=1.297$ ), although with a clear enrichment for significant associations compared to the null. We therefore chose to apply a more stringent multiple testing correction to ensure robust associations in the PCGC cohort.

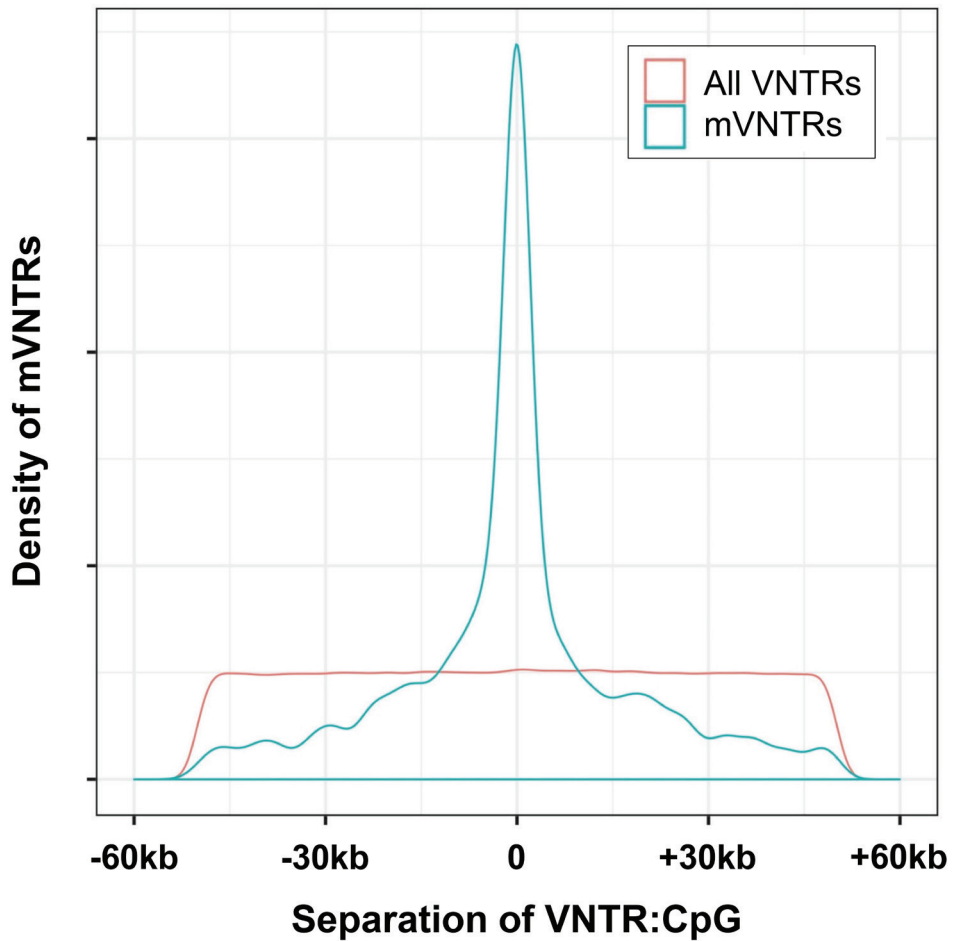


**Figure S10. Significant mVNTRs show strong enrichments to be located within close proximity to the CpG whose methylation level they are associated with.** These results mirror similar observations made for SNV mQTLs,<sup>65</sup> and for eVNTRs in the GTEx cohort (Figure 1E). However, we note an approximate order of magnitude difference in the distances over which significant eVNTRs and mVNTRs were typically observed to function.

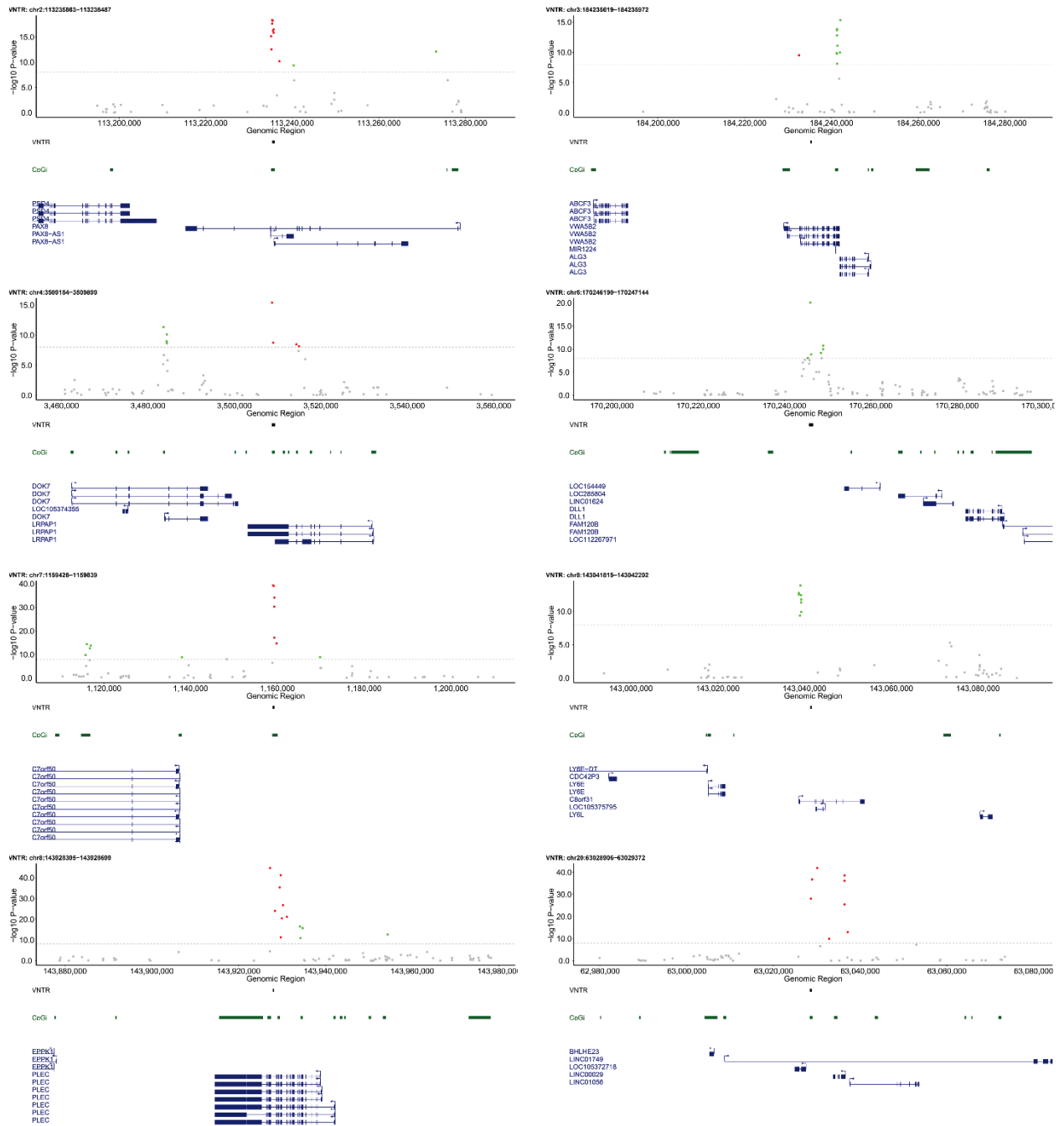


**Figure S11. Eight example mVNTR loci detected in the PGC cohort.** Each plot shows associations between copy number of a VNTR and CpG methylation within  $\pm 50$ kb (hg38 coordinates). The horizontal dashed line indicates the significance threshold ( $p < 0.01$  after Bonferroni correction for the number of pairwise tests performed genome-wide), with significant

CpGs shown in color, with red representing positive correlations with VNTR copy number, and green indicating negative correlations. The location of the VNTR is indicated by the horizontal black bar in the center below each plot. Underneath each plot are shown the location of CpG islands (green bars) and Refseq genes (blue).

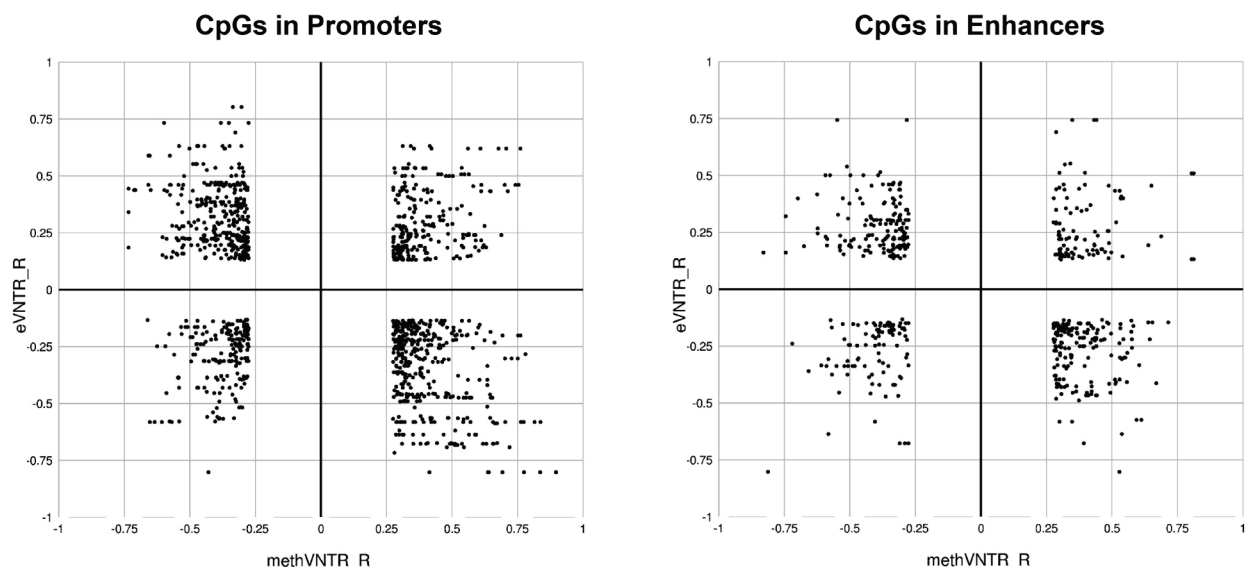


**Figure S12. An inverse relationship between gene expression and methylation of regulatory elements associated with VNTRs.** Considering VNTRs that were associated with both methylation of CpGs in annotated regulatory regions and expression of the genes they regulate, we compared the correlation coefficients between VNTR copy number and both methylation and expression. We observed that for both promoters ( $p=5.8 \times 10^{-10}$ ) and enhancers ( $p=3.9 \times 10^{-16}$ ) there was a significant inverse relationship of CpG methylation with gene expression, *i.e.* functional VNTRs preferentially showed opposite directionality of effects on methylation of regulatory elements and expression of the associated genes.

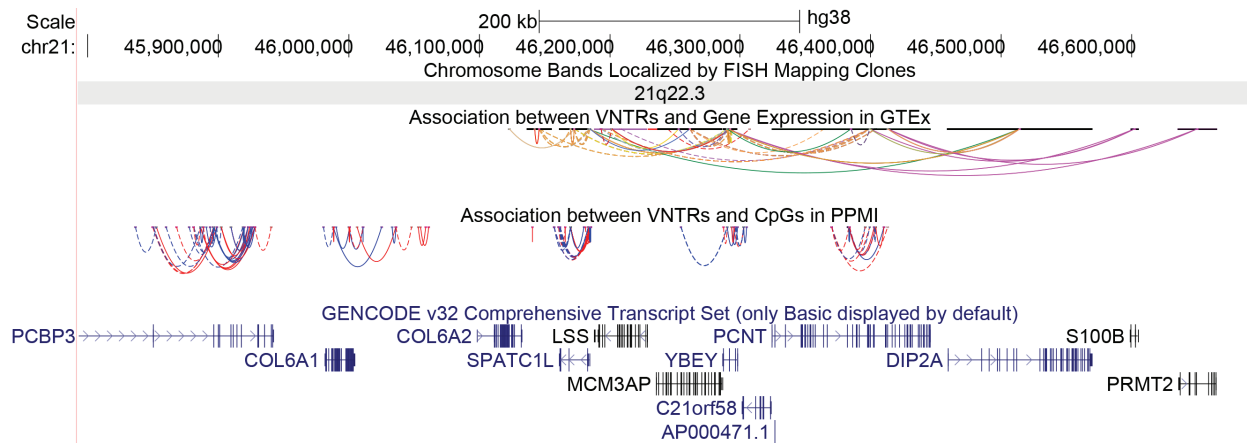


**Figure S13. Screenshot showing UCSC Genome Browser tracks created to display eVNTRs and mVNTRs identified in our analysis.** Shown is an example region of ~900 kb located at 21q22.3. Each line joins the location of an eVNTR:gene transcription start site, or mVNTR:CpG pair. For GTEx eVNTRs, line color indicates tissue type, while for mVNTRs blue and red lines represent positive and negative associations, respectively. Tracks are titled “Exp/Meth VNTR hub” accessible via the UCSC Genome Browser Track Hubs for both the hg19 and hg38 genome assemblies. A link is included in the Data and Code Availability section of the manuscript.

## Acknowledgements

This work was supported by NIH grant NS105781 to AJS, NIH grant R01HG010485 to BP, NIH predoctoral fellowship NS108797 to OLR, and American Heart Foundation Postdoctoral Fellowship 18POST34080396 to AMT. Research reported in this paper was supported by the Office of Research Infrastructure of the National Institutes of Health under award number S10OD018522. The content is solely the responsibility of the authors and does not necessarily represent the official views of the National Institutes of Health. This work was supported in part through the computational resources and staff expertise provided by Scientific Computing at the Icahn School of Medicine at Mount Sinai.

The Genotype-Tissue Expression (GTEx) Project was supported by the Common Fund of the Office of the Director of the National Institutes of Health ([commonfund.nih.gov/GTEx](http://commonfund.nih.gov/GTEx)). Additional funds were provided by the NCI, NHGRI, NHLBI, NIDA, NIMH, and NINDS. Donors were enrolled at Biospecimen Source Sites funded by NCI\Leidos Biomedical Research, Inc. subcontracts to the National Disease Research Interchange (10XS170), Roswell Park Cancer Institute (10XS171), and Science Care, Inc. (X10S172). The Laboratory, Data Analysis, and Coordinating Center (LDACC) was funded through a contract (HHSN268201000029C) to the The Broad Institute, Inc. Biorepository operations were funded through a Leidos Biomedical Research, Inc. subcontract to Van Andel Research Institute (10ST1035). Additional data repository and project management were provided by Leidos Biomedical Research, Inc.(HHSN261200800001E). The Brain Bank was supported supplements to University of Miami grant DA006227. Statistical Methods development grants were made to the University of Geneva (MH090941 & MH101814), the University of Chicago (MH090951, MH090937, MH101825, & MH101820), the University of North Carolina - Chapel Hill (MH090936), North Carolina State University (MH101819), Harvard University (MH090948), Stanford University (MH101782), Washington University (MH101810), and to the University of Pennsylvania

(MH101822). The datasets used for the analyses described in this manuscript were obtained from dbGaP at <http://www.ncbi.nlm.nih.gov/gap> through dbGaP accession number phs000424.v7.p2.

The Gabriella Miller Kids First Pediatric Research Program (Kids First) was supported by the Common Fund of the Office of the Director of the National Institutes of Health ([www.commonfund.nih.gov/KidsFirst](http://www.commonfund.nih.gov/KidsFirst)). Baylor College of Medicine's Human Genome Sequencing Center was awarded an administrative supplement (3U54HG003273-12S1) to sequence congenital cohort samples submitted by Christine Seidman through the Kids First program (1X01HL132370). The data analyzed and reported in this manuscript were accessed from dbGaP ([www.ncbi.nlm.nih.gov/gap](http://www.ncbi.nlm.nih.gov/gap); accession number phs001138). Additional funds from the NHLBI grants U01HL098123, U01HL098147, U01HL098153, U01HL098162, U01HL098163, and U01HL098188 supported the assembly of the Pediatric Cardiac Genomics Consortium (<https://benchtopassinet.com/About/AboutPCGC>) cohort, and collection of the phenotypic data and samples (PMID: 23410879).

Data used in the preparation of this article were obtained from the Parkinson's Progression Markers Initiative (PPMI) database ([www.ppmiinfo.org/data](http://www.ppmiinfo.org/data)). For up-to-date information on the study, visit [www.ppmiinfo.org](http://www.ppmiinfo.org). PPMI, a public-private partnership, is funded by the Michael J. Fox Foundation for Parkinson's Research and funding partners, a full list of which can be found at [www.ppmiinfo.org/fundingpartners](http://www.ppmiinfo.org/fundingpartners).

WGS data for samples from the 1000 Genomes Project sample collection were generated at the New York Genome Center with funds provided by NHGRI Grant 3UM1HG008901-03S1.